Grid and Rotor Sides of Doubly-fed Induction Generator-based Wind Energy Conversion System Using Sliding Mode Control Approach

by

Hisham Salem Ali Eshaft

A thesis submitted to
Saint Mary's University, Halifax, Nova Scotia,
in partial fulfillment of the requirements for
the degree of Master of Science in Applied Science

August 2017, Halifax, Nova Scotia

Approved: Dr. Adel Merabet
Supervisor
Division of Engineering

Approved: Dr. Bashir Khan
Member Supervisory Committee
Mathematic & Computing Science Department

Approved: Dr. Jason Rhinelander
Member Supervisory Committee
Division of Engineering

Approved: Dr. Amer Ghias
External Examiner
Electrical and Computer Engineering
University of Sharjah, United Arab Emirates

Date: August 8, 2017

Abstract

Grid and Rotor Sides of Doubly-fed Induction Generator-based Wind Energy Conversion System Using Sliding Mode Control Approach

by Hisham Eshaft

Abstract

This thesis deals with the analysis, modeling, and control of a Doubly-Fed Induction machine used as a wind turbine generator. A sliding mode control scheme is applied to control the power and Dc-link voltage. Two back-to-back converters are used at rotor and stator sides. At the rotor side, power control is achieved by controlling the rotor current, while at the grid side, an active power transfer is used to model the dc-link voltage. Overall robustness and tracking performance are enhanced to deal with uncertainties due to the structure of the sliding mode control law, compensation combinations, sliding and integral terms. An experimental 2-kw DFIG wind turbine system was used to validate the proposed control system. Based on the results obtained, the proposed system showed good capabilities in tracking and control under various operating conditions as well as robustness to uncertainties.

August 8,

2017.

Acknowledgement

I would like to express my sincere gratitude to my supervisor, Dr. Adel Merabet, for his constant guidance, time spent with me, and valuable advice, all of which helped bring this work to a successful conclusion. As well, I would like to thank my supervisory committee members, Dr. Jason Rhinelander, Dr. Bashir Khan, and the external examiner, Dr. Amer Ghias for their helpful comments and suggestions. I would also like to thank the entire research group of the Laboratory of Control Systems and Mechatronics (LCSM), Division of Engineering, at Saint Mary's University, for their support and assistance.

Finally, I must express my very profound gratitude to my parents and to my spouse for providing me with unfailing support and continuous encouragement throughout my years of study, and through the process of researching and writing this thesis. All of these accomplishments would not have been possible without them.

Table of Contents

List of Illustration

List of Abbreviation

Acronyms	Description
IM	Induction Machine
DFIM	Doubly Fed Induction Machine
DFIG	Doubly Fed Induction Generator
SCIG	Squirrel Cage Induction Generator
kW	Kilo Watt
GW	Giga Watt
PWM	Pulse Width Modulation
DPC	Direct Power Control
DTC	Direct Torque Control
PDPC	Predictive Direct Power Control
PDTC	Predictive Direct Torque Control
IVS-DTC	Integral Variable Structure-Direct Power Control
AVR/PSS	Automatic Voltage Regulator/Power System Stabilizer
FRT	Fault Ride Through
IGBT	Insulated Gate Bipolar Transistor
FPGA	Field Programmable Gate Array
PI	Proportional Integral
RTS	Real Time Simulation
RCP	Rapid Control Prototyping

HIL	Hardware in the Loop
PS	Pure Simulation

Acronyms	Description
WT	Wind Turbine
WECS	Wind Energy Conversion System
SMC	Sliding Mode Controller

Chapter 1

Introduction

1.1. Background and Motivation

Renewable energy resources have gained significant attention of the industry and the academic researcher, because it is environmentally friendly [1], [2], [3]. Wind turbines usually operate under variable speed operation to provide efficient energy, with the power extracted contributing a significant proportion of consumers' electrical power demands. In fact, 20% of the entire electricity consumption in Denmark is now provided by wind energy [4]. In recent years, several different power converter techniques have been developed to integrate wind turbines with the electrical grid. The use of electronic power converters allows for variable speed operation of wind turbines as well as enhanced power extraction. In variable speed operation, a control method is required that extracts maximum power from the turbine while providing constant grid voltage and frequency. A wide range of control schemes, varying in cost and complexity, have been investigated for previously considered conversion systems.

All of the control schemes integrated with power electronic converters are designed to maximize power output at every possible wind speed. These speeds can range from cut-in to rated, and are specific to the size and type of generator being used in the Wind Energy Conversion System (WECS) [5]. A WECS based on Doubly Fed Induction Generator DFIG has several advantages [6]. For instance, it decreases stress on the mechanical structure, reduces acoustic noise, and offers the possibility of regulating both active and reactive power by using classical d-q control method [7]. Another advantage of

a DFIG system is that the back-to-back Pulse Width Modulation PWM converters connected between the grid and the induction machine rotor circuit are sized for only a portion (approx. 30%) of the generator's full power. Wind turbine generators (WTGs) can achieve maximum wind power provided at various wind speeds by correctly adjusting the shaft speed [7].

One of the most common control techniques is decoupling the PI control of the output active and reactive power to improve the dynamic behavior of wind turbines. However, due to uncertainties surrounding the modeling and behavior of some parameters (e.g., wind speed, wind turbines, and differences in parameter values during operation due to extreme or variable temperatures, unpredictable wind speeds, or other events), the tuning of PI is a challenge in the classical d-q control scheme [8].

In the formulation of any practical control problem, there will always be a discrepancy between the actual plant and its mathematical model used for the controller design. These discrepancies (or mismatches) arise from unknown external disturbances, plant parameters, and parasitic/unmodeled dynamics [9]. Designing control laws that provide the desired performance to the closed-loop system in the presence of these disturbances and uncertainties is a very challenging task for a control engineer. This has led to intense interest in the development of the so-called robust control methods which are supposed to solve this problem.

One approach to robust controller design is the so-called sliding mode control scheme [9]. The advantages of using a sliding mode controller are its simple control structure and its insensitivity to model imprecision caused by unknown disturbances and variations in parameters [10]. In the industry, Proportional (P), Proportional Integral (PI) and

Proportional Integral Derivative (PID) controllers are widely used due to their simple structures and ease of use in a wide range of applications.

However, these controllers are tuned for specific linearized models. They may provide insufficient performance for different operating points caused by disturbances and parameter uncertainties, leading to undesirable and sustained oscillations in power and voltage. Furthermore, large and slow wind deviations may even lead to system instability [11]. To obtain maximum power extraction, the four types of electrical configuration for wind energy conversion systems should be considered.

As summarized in Fig. 1.1, there are generally four accepted electrical configurations for wind energy conversion systems currently in use. Type 1 and Type 2 illustrate the configurations for a fixed-speed wind turbine, and Type 3 and Type 4 illustrate those for a variable-speed wind turbine. In a fixed-speed wind turbine, the generator is directly connected to the electrical grid, whereas in a variable-speed wind turbine, the generator is controlled by powered electronic equipment. There are several advantages in using variable-speed wind turbines, including decreased stress on the mechanical structure, reduced acoustic noise, and the ability to control power and Dc-link voltage [12]. Most major wind turbine manufactures are now developing wind turbines in the 3-to-6-MW range [13]. These large wind turbines are all based on variable-speed operation with pitch control using a direct-driven synchronous generator (without gear box) or a doubly-fed induction generator. Fixed-speed induction generators with stall control are regarded as unfeasible [13] for large wind turbines. Today, variable-slip (i.e., where the slip of the induction machine is controlled with external rotor resistances) or

doubly-fed induction generators are most commonly used by the wind turbine industry for larger wind turbines [14].

Among the four major electrical configurations mentioned above, Type 3 and Type 4 using induction generators are the most common configurations. Nevertheless, these configurations contribute reactive power generation as well as active power. In Type 4, the generated power at stator terminals converts DC power and is injected to the grid using a DC/AC converter. In this case, the entire generated power passes through the switching components, which typically results in power losses of up to 10%. However, Type 3, with doubly-fed induction generators (DFIG) using wound rotor-type asynchronous machines, offers a more efficient solution, as only 30% of the total system power [13, 14, 15] passes through the rotor-side converter and the stator is directly connected to grid. This means that the losses in the power electronic equipment will be reduced in comparison to power electronic equipment that has to handle the total system power, such as a direct-driven synchronous generator (Type 4). There is also a cost saving in using a smaller converter.

As a result of its reduced power delivery through power electronic devices, Type 3's size would be smaller and its power loss and converter cost would be much lower than in Type 4. Less power dissipation also means lower cooling expenses. So, it is more cost-effective to choose the Type 3 configuration, as the stator connects directly to the grid [16, 17, 18, 19]. However, there are some concerns about the operational difficulties of the machine in instances of grid voltage disturbances. Although a variety of control methods exist, the importance and novelty of the DFIG concept means that different control methods in rotor-side and grid-side converters and their effects on the performance of wind power generators need to be investigated.

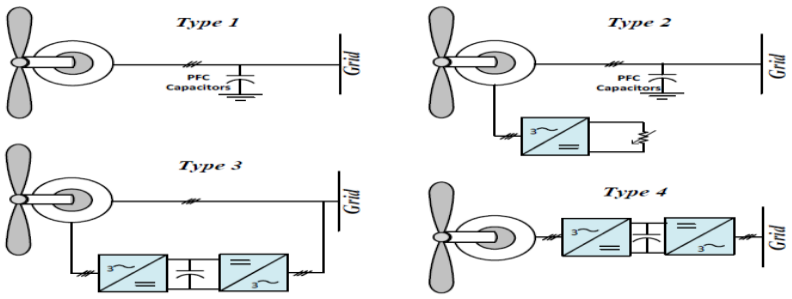

Fig.1.1: Various types of wind energy conversion system models [14].

1.2. Literature Review

The use of doubly-fed induction generators (DFIGs) is advantageous, since they are relatively inexpensive, robust and require low maintenance. Furthermore, because they require external reactive power support from the grid, DFIGs need bi-directional power flow in the generator-side converter in order to inject the power when it needs to consume the reactive power and balanced with grid [20]. The use of back-to-back PWM converters along with the implementation of sliding mode controllers is a consistent converter-control combination which is carried out from the hardware system. Meanwhile, the method of commutating to control the hardware system is attracting the trajectory state to the switching surface during the convergence mode [21]. Some controllers that can induce asymptotically stable sliding behaviors of any order have been presented in the literature [22, 23, 24]. However, in [25, 26], we find the first generation of specifically designed controllers that give rise to finite time second-order sliding behaviors in a time-varying sliding surface VSS. The VSS is a special class of nonlinear systems characterized by a discontinuous control action which changes structure upon reaching a set of sliding surfaces. A salient property of the VSS system is the sliding motion of the state on the sliding surface. During this sliding motion, the system has invariance properties yielding motion which is independent of certain parameter uncertainties and disturbances.

Therefore, the design of the sliding surface completely determines the performance of the system. Most of the sliding surfaces proposed so far have been designed without consideration of the initial conditions, whether given or arbitrary. Using these sliding surfaces, the sliding mode occurs only after the system reaches the surfaces. Therefore, the tracking behaviors can be hindered by the uncertainties especially during the reaching phase. In [27], the mechanical dynamics method of the second-order sliding was implemented to control the power of wind turbines and to extract the maximum power of the wind turbine, with the sliding mode being applied to track the torque [28]. Speed was controlled by implementing the sliding mode method to the rotor speed dynamics [29] and [30]. In [31], we see a combination of sliding mode-based field-oriented control and an observer to control the aerodynamic torque.

The rotor slots interact with the magnetizing component of the air-gap magneto-motive force (MMF), generating harmonics that are dependent on the machine's rotational speed. Once the algorithm locates the frequency of the rotor slot harmonics RSH through a look-up table, the rotational speed can be found through a series of calculations. More information on this system is located in [32], which indicates that the control option for the supply-side converter includes controlling active and reactive power. A reference frame orientated along the supply voltage rotating vector allows for real power control through d-axis current control and q-axis manipulation controls the reactive power. The aforementioned control is proven to track fast changes in rotational speed with high accuracy, a favorable characteristic for systems employing a stall- controlled wind turbine. This control algorithm can react quickly to wind gusts and may be utilized to control the amount of mechanical power and torque input to the generator. These are

common concerns for stall-controlled wind turbines, as operating them over the rated power may cause damage to the generator and power electronic converter [32].

A comparison between the use of a wound rotor induction machine and a caged rotor induction machine, both of identical size, was performed in [33]. Each of the induction machines had six poles and were rated with a voltage of 415 V 300kW and a speed of 1000 RPM. The comparison ensures validity with the use of identical converter types in each of the systems. The separate designs were each tested under identical variable wind conditions. Under the same conditions, the wound rotor induction machine output 35kWh of energy over 10 min, whereas the caged induction machine only output 28.5kWh in 10 min. The higher cost of the wound rotor induction machine, due to possible need for slip rings, is compensated by the reduction in the size of the power converters and thus the increase in energy efficiency.

The idea of using wound rotor induction machines was introduced when the doubly-fed generation was implemented for reluctance machines [33, 34, 35]. The first practical use of DFIG is recorded by Pena et al. [36], where the control strategy was based only on PI controllers connected with sinusoidal PWM that resulted in a constant switching frequency. The authors in [37] illustrated the detailed model-based studies on DFIG, showing how the rotor position can be found through current and voltage models. Another model was recorded in [38], where the operation of the DFIG under voltage sag was studied. Further studies on transient analysis of DFIG followed in [39]. The use of a hysteresis current controller on DFID to achieve better dynamics was reported in [40].

The DFIG uses two back-to-back converters connected to a three-phase power supply to deliver the required magnetization current at rotor side. In fact, one of the three-phase converters is connected to the grid to provide stable DC voltage. This converter is usually

called a grid-side converter (GSC). The DC voltage can be used for another voltage source for three-phase converters which is directly connected to terminals of a rotor winding, called a rotor-side converter (RSC). RSCs have the same configuration as GSCs, the only difference is in the control strategy when compared to the GSC one. The main task of a GSC is not only to keep the dc bus voltage constant, but also to compensate the reactive power or in some cases to remove reactive power disturbance during unbalanced conditions [41]. The main purposes of an RSC is to provide the required magnetization in rotor windings in order to generate the necessary active and reactive power at stator terminals. However, it has been reported in under some control methods [42], the active and reactive reference values have been substituted with the values of the electrical torque and stator flux.

The need to increase the efficiency of the machine to meet the new grid codes for fault ride through performance led to further studies [43, 44]. Some control strategies were proposed to improve the fault ride capability of wind turbine generators in case of short-circuiting or unbalanced condition situations, as reported in the literature. Examples include direct active control methods [45], model-based studies [46, 47], predictive direct power control PDPC [48, 49], predictive direct torque control DTC [50], vector-based hysteresis [51, 52], and integral variable structure direct torque control IVS-DTC [53]. Additionally, sensorless methods, which are known for their reliability, immunity to noise and cost-effectiveness, have also been reported by previous researchers [54, 55, 56, 57], and a comparative study for some basic control approaches was performed [58].

The major disadvantage of the aforementioned works is their deficiency in coping with large changes in grid-side parameters. Despite some useful hints for hardware setup

that have been reported in previous research, there is not enough detailed design documented in the literature. For this reason, studying DFIG through practical implementation would help to justify various methods and ideas. As most of the control methods use PI to control the inner loop, a new improved technique was applied, known as the sliding mode control scheme.

1.3. Objective

The main purpose of this thesis is the analysis of the DFIG for a wind turbine (WT) application during steady-state operation of 2kW DFIG based wind energy conversion system emulator. In order to analyze the DFIG during steady-state and transient operation both the modeling and the control of the system is important. Hence, the control and the modeling are also important parts of the thesis. The main contribution of this thesis is dynamic and steady-state analysis of the DFIG, as follows

i- To develop a power control-based sliding mode approach for a DFIG-wind energy conversion system for a rotor-side convertor

ii- To develop a sliding mode control for Dc-link voltage regulation and to improve the power quality in a grid-side converter.

iii- To validate the proposed control scheme on the hardware prototype of DFIG-WECS. and verify its tracking efficiency and robustness.

1.4. Development Steps:

i. Development control scheme for DFIG-based WECS
   a. Sliding mode controllers for rotor side
   b. Sliding mode controller grid side
ii. Development of supervision and control interface

iii. Experimental validation

1.5. Outline

This thesis is organized as follows:

In **Chapter 2**, Description of properties of the wind and wind energy conversion system. Overview of Doubly Fed Induction Generator (DFIG) based wind turbine and the dynamic modeling of DFIG in stationary & rotating reference frame for the development of machine control are presented

In **Chapter 3**, The main work in chapter is to develop an SMC scheme, where a switching term, an integral term and a compensating term can all be included to efficiently operate a DFIG-based WECS and deal with uncertainties, parametric mismatches and external disturbances. The control scheme will be used to ensure that the active-reactive power at the generator stator is regulated on a constant basis and to maintain a continuous dc-link voltage at the back-to-back convertor.

In **Chapter 4**, an analysis of the graphical representation of system performances is provided, obtained by real-time experiments and offering practical information as well as a deeper understanding of the machine's behavior in a wind energy conversion system.

Finally, in **Chapter 5**, the conclusion and proposed future work are presented.

Chapter 2

Dynamic Modeling of Wind Turbine and DFIG

2.1. Wind Turbine

A wind turbine is one of the most important elements in wind energy conversion systems. Wind turbines produce electricity by using the power of the wind to drive an electrical generator. The wind passes over the blades, generating lift and exerting a turning force, while the rotating blades turn a shaft inside the nacelle that goes into a gearbox. The gearbox increases the rotational speed to whatever speed is appropriate for the generator, and the generator then uses magnetic fields to convert the rotational energy into electrical energy. Finally, the power output goes to a transformer or power electronic converter, which converts the electricity from the generator by regulating the voltage.

Wind turbines extract kinetic energy from the swept area of the blades. The power in the airflow is given by [59], [60].

$$P_{air=}\frac{1}{2}\rho A v^3 \tag{2.1}$$

where

ρ = Air density (kgm^{-3})

A = Swept area of rotor (m^2)

v = Wind speed (ms^{-1})

Although the above equation gives the power available in the wind, the power transferred to the wind turbine rotor is reduced by the power coefficient, C_p [59]:

$$C_p = \frac{P_{wind\ turbine}}{P_{air}} \tag{2.2}$$

$$P_{wind\ turbine} = C_p P_{air} = P_M \quad (2.3)$$

The wind power captured by the blade and converter into mechanical power, (P_M), can be calculated by:

$$P_{wind\ turbine} = P_M = C_p \times \frac{1}{2} \rho A v^3 \quad (2.4)$$

$$P_M = \frac{1}{2} \rho \pi R^2 v^3 C_p \quad (2.5)$$

The maximum value of C_p is defined by the Betz limit, which states that a turbine can never extract more than 59.3% of the power from an air stream [59] [61]. In reality, wind turbine rotors have maximum C_p values in the range of 25% to 45%. It is also conventional to define a tip-speed ratio, λ, as

$$\lambda = \frac{\omega R}{v} \quad (2.6)$$

where ω = rotational speed of rotor

R = radius to tip of rotor

ν = upwind free wind speed, ms^{-1}

The tip-speed ratio, λ, and the power coefficient, Cp, are dimensionless and thus can be used to describe the performance of any size of wind turbine rotor. Wind turbines can rotate about either Horizontal Axis Wind Turbines HAWT or Vertical Axis Wind Turbines VAWT (Darius, Savonius) [62].

Horizontal Axis Wind Turbines

HAWTs, which are mounted on towers, are the most common type of turbine (Fig. 2.1). Their main advantages are high efficiency and low cost/power ratio, while their drawbacks are complex design and maintenance difficulties, as both the generator and gearbox must be tower-mounted.

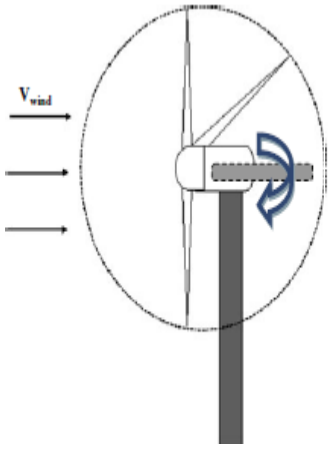

Figure 2.1: Horizontal Axis Wind Turbine

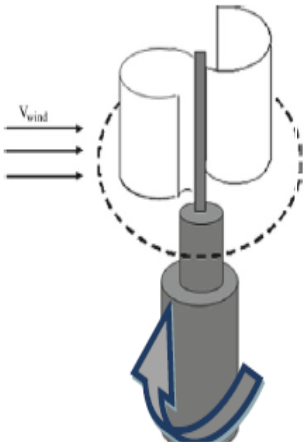

Figure 2.2: Savonius Vertical Axis Wind Turbine

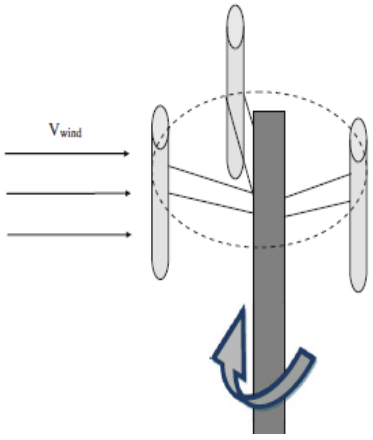

Figure 2.3 Darius Vertical Axis Wind

The first windmills built (Savonius rotor [Fig. 2.2] and Darius rotor [Fig. 2.3]) were based on a vertical axis structure. In VAWT, the maintenance is easy and wind can be received from any direction. Furthermore, the VAWT blade design is simple and has low fabrication costs. The main drawbacks of VAWT are that it requires a generator to run in motor mode at startup and has lower oscillatory components in the aerodynamic torque [62]. The mechanical connection between an electrical generator EG and turbine rotor may be direct or through a gearbox. In fact, the gearbox (G) converts the turning speed of the blades, ω_t, to the rotational speed, ω_g, of an electrical generator (EG) [63]:

$$\omega_t = \frac{\omega_g}{G}$$

We defined the tip speed ratio (TSR) for wind turbines as the ratio of the rotational speed of the tip of a blade, $\omega_t . R$, to the actual wind speed, V_{wind} :

$$\lambda = \frac{\omega_t . R}{V_{wind}}$$

Modern horizontal axis wind turbines generally use k (constant number) of nine-to-ten for two-bladed rotors and six-to-nine for three-bladed rotors.

2.2. Dynamic Modeling of Doubly-fed Induction Generator

Induction machines (IMs) have been widely used as a means of converting electric power to mechanical work in several applications. The main advantage of an IM is that there is no need for separating DC field power because of its brushless construction. These machines are known for their reliability and can be found in the ranges of fractional horse power (FHP) to multi-megawatt capacity. Moreover, unlike synchronous machines, IMs can be operated at different speeds. There are two types of induction machines, based on rotor construction: squirrel cage rotor and wound rotor. The squirrel cage rotor type is widely used because of its simplicity of construction and low maintenance cost, whereas the wound rotor machine is usually used as a grid-connected choice because the reactive power could be injected to the grid through rotor winding to balance the power at the grid and it can also produce high starting torque. The squirrel cage is the preferred option in stand-alone wind generation schemes, as it can produce a higher starting torque than DFIG [64].

The dynamic behaviors of the induction machine must be tested as the modeling is done to study dynamics. Dynamic behavior illustrates the behavior of the machine's variables in transition periods as well as in the steady state. This dynamic behavior of machines is known as the "dynamic model". By using the dynamic model, the performance of the machine parameters can be known for all stages of operation (not only steady-state) such as torque, currents and fluxes, as well as under certain voltage-supplying conditions [65]. Furthermore, the information provided by the dynamic model helps to show how the

transition from one state to another is achieved, and allows for the detection of instabilities or high transient currents that are considered unsafe behaviors. [65].

Therefore, the dynamic model is represented in a differential equation form and structured as a compact set of model equations. This allows it to be simulated using any control software such as Simulink-MATLAB and RT-LAB. The set provides all the relevant information related to the machine's variables, along with the behavior of the variables of the machine.

2.2.1. Overview of Doubly-fed Induction Generator

DFIG is known as a wound rotor induction generator. Both the stator and the rotor have three sinusoidal windings, corresponding to three phases, displaced by 120^{o}. The three phases are *a*, *b* and *c*, while the stator has *p* pairs of poles.

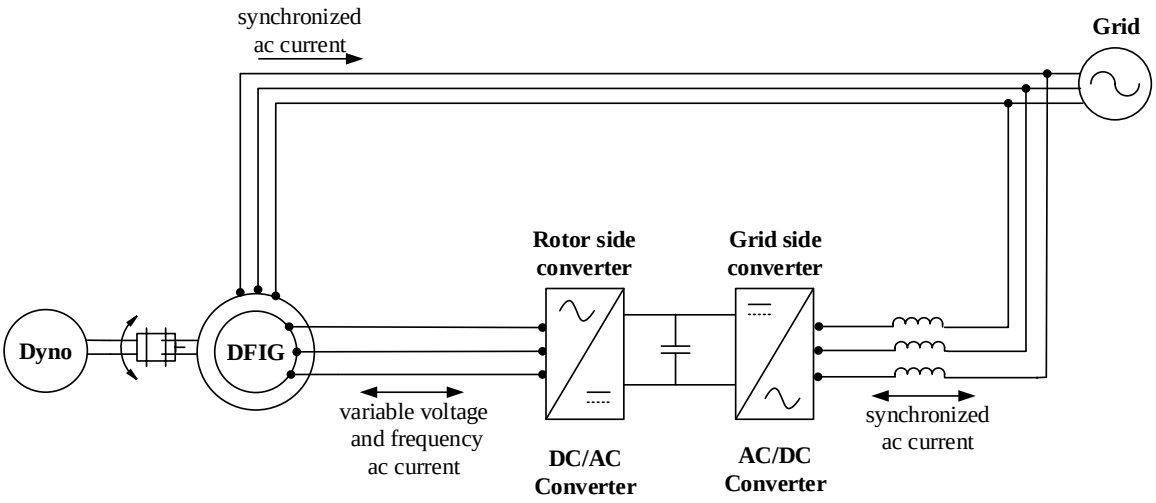

Figure 2.4: Schematic of DFIG configuration.

The rotor is connected to the grid through AC/DC converters, as shown in Fig. 2.4. When the machine produces energy, 30% of the power flows from the rotor to the grid. The design of the converters can then be chosen in accordance with the rotor's power. The minimization of the converter volume and cost is assured, unlike the squirrel cage induction

generator, where the converter must handle the full load power, significantly increasing the cost of the assembly.

The stator windings are connected to the grid. This imposes the stator current frequency, f_e, and leads to the creation of a rotating magnetic field in the air gap. The relationship between the rotational speed of this field, ω_e and f_e , is proportional:

$$\omega_e = 2\pi f_e. \tag{2.7}$$

The variation of magnetic flux appears when the rotor speed is different than the speed of the rotational field. Currents are induced in the rotor windings in accordance with Faraday's law of induction. Hence, we can define P is number of poles, ω_m, the rotor mechanical speed and, ω_r, the rotor electrical speed by

$$\omega_r = P\omega_{m.} \tag{2.8}$$

If $\omega_r \neq \omega_e$, the flux linked by the rotor windings will change with time; whereas if $\omega_r > \omega_e$, the machine will be operated as a generator and as a motor otherwise, the DFIG could be operated as a generator in sub-synchronous mode. The slip, s, defines the relative speed of the rotor compared with the relative speed of the stator:

$$s = \frac{\omega_e - \omega_r}{\omega_e} \tag{2.9}$$

The slip of DFIG is usually negative when it works as a generator and positive when it works as motor. The rotor currents at an angular speed are defined by the difference between the synchronous speed and the rotor speed, whereas the stator currents at ω_r are defined by $\omega_e - \omega_r$.

This means that the frequency of the rotor currents, f_r, is [65]

$$f_r = s\, f_e. \tag{2.4}$$

The machine should be always operated at speeds different from synchronous speed in order to detect changes in the magnetic flux, which leads to inducing currents in its winding.

The rotor-side inverter controls the rotor currents. Equation (2.4) illustrates how controlling the rotor currents controls both the slip and the speed of the machine.

2.2.2. Doubly-fed Induction Generator Modeling

The mathematical modeling of the DFIG is presented in this section. In order to provide the needed feedback to tune the controller, the electrical equivalent of the DFIG is illustrated and analyzed. Moreover, all equations of the equivalent system are transformed into both an αβ and a dq0 reference frame. Furthermore, the decoupled active and reactive power equations are exposed in the d and q axes for both the stator and the rotor.

In the stationary (*abc*) reference frame, the relationships between voltages, currents and flux linkages of each phase of the machine can be obtained by Kirchhoff's and Faraday's laws [66-67]:

$$\begin{bmatrix} v_{as} \\ v_{bs} \\ v_{cs} \end{bmatrix} = R_s \times \begin{bmatrix} i_{as} \\ i_{bs} \\ i_{cs} \end{bmatrix} + \frac{d}{dt} \begin{bmatrix} \lambda_{as} \\ \lambda_{bs} \\ \lambda_{cs} \end{bmatrix} \tag{2.10}$$

$$\begin{bmatrix} v_{ar} \\ v_{br} \\ v_{cr} \end{bmatrix} = R_r \times \begin{bmatrix} i_{ar} \\ i_{br} \\ i_{cr} \end{bmatrix} + \frac{d}{dt} \begin{bmatrix} \lambda_{ar} \\ \lambda_{br} \\ \lambda_{cr} \end{bmatrix} \tag{2.12}$$

The subscripts *r* and *s* denote rotor and stator quantities, respectively. The subscripts *a, b* and *c* are used to identify phases *a, b* and *c* quantities, respectively. The

symbols *v* and *i* are for voltages and currents, and λ represents flux linkages. The stator and rotor winding resistances are R_s and R_r. They are assumed to be equal for all phase windings.

The flux linkages are coupled to the currents by the inductances:

$$\begin{bmatrix} \lambda_{as} \\ \lambda_{bs} \\ \lambda_{cs} \end{bmatrix} = L_s \begin{bmatrix} i_{as} \\ i_{bs} \\ i_{cs} \end{bmatrix} + L_M \begin{bmatrix} i_{ar} \\ i_{br} \\ i_{cr} \end{bmatrix} \tag{2.13}$$

$$\begin{bmatrix} \lambda_{ar} \\ \lambda_{br} \\ \lambda_{cr} \end{bmatrix} = L_r \begin{bmatrix} i_{ar} \\ i_{br} \\ i_{cr} \end{bmatrix} + L_M^T \begin{bmatrix} i_{as} \\ i_{bs} \\ i_{cs} \end{bmatrix} \tag{2.14}$$

The winding inductance matrices are defined by:

$$L_s = \begin{bmatrix} L_{ls} + L_m & -\frac{1}{2}L_m & -\frac{1}{2}L_m \\ -\frac{1}{2}L_m & L_{ls} + L_m & -\frac{1}{2}L_m \\ -\frac{1}{2}L_m & -\frac{1}{2}L_m & L_{ls} + L_m \end{bmatrix} \tag{2.15}$$

$$L_r = \begin{bmatrix} L_{lr} + L_m & -\frac{1}{2}L_m & -\frac{1}{2}L_m \\ -\frac{1}{2}L_m & L_{lr} + L_m & -\frac{1}{2}L_m \\ -\frac{1}{2}L_m & -\frac{1}{2}L_m & L_{lr} + L_m \end{bmatrix} \tag{2.16}$$

$$L_M = L_m \begin{bmatrix} \cos(\theta_r) & \cos(\theta_r + \frac{2\pi}{3}) & \cos(\theta_r - \frac{2\pi}{3}) \\ \cos(\theta_r - \frac{2\pi}{3}) & \cos(\theta_r) & \cos(\theta_r + \frac{2\pi}{3}) \\ \cos(\theta_r + \frac{2\pi}{3}) & \cos(\theta_r - \frac{2\pi}{3}) & \cos(\theta_r) \end{bmatrix} \tag{2.17}$$

The subscripts *l* and *m* relate to the leakage and magnetizing inductances, respectively. The maximum amplitude of the mutual inductance between the stator and the

rotor is L_m. It should also be noted that Eq. (2.7) depends on the angular shift of the rotor, θ_r, which in turn depends on the angular speed of the rotor, ω_r. The rotor electrical angular displacement regarding the stator, defined from ω_r, of the electrical rotor speed is

$$\theta_r(t) = \int_0^t \omega_r dt + \theta_r(t) \tag{2.18}$$

where θ_r (0) is the initial position of the rotor at t=0.

It can then be noted that the voltage, current and mutual inductance matrix, L_M, are derived in the (*abc*) stationary reference frame and depend on time. Since the modeling and analysis for such a system is difficult to manage, the time-variant parameters can be made time-invariant by transforming them into an appropriate rotating reference frame.

In order to complete the modeling, a model of the mechanical dynamics is needed. The dynamics of the generator shaft relate the rotor speed and the electromagnetic torque:

$$J\frac{d\omega_m}{dt} = T_m - T_e \tag{2.19}$$

where J is the inertia of the machine, T_m is the mechanical torque, and T_e is the electromagnetic torque.

2.2.3. (*d-q*) Reference Frame

It has been mentioned above that the parameters of the machine need to be transformed into a suitable rotating reference frame. This aim can be achieved by defining the (*d-q*) reference frame, which will be rotating at the synchronous angular speed of the system. The DFIG can be considered a generator with a non-zero rotor voltage. Hence, the equations for the rotating direct-quadrature (*d-q*) reference frame can be written as [68]:

$$v_{ds} = R_s i_{ds} - \omega_e \lambda_{qs} + \frac{d\lambda_{ds}}{dt} \tag{2.20.a}$$

$$v_{qs} = R_s i_{qs} + \omega_e \lambda_{ds} + \frac{d\lambda_{qs}}{dt} \quad (2.20.b)$$

$$v_{dr} = R_r i_{dr} - \omega_s \lambda_{qr} + \frac{d\lambda_{dr}}{dt} \quad (2.21.a)$$

$$v_{qr} = R_r i_{qr} + \omega_s \lambda_{dr} + \frac{d\lambda_{qr}}{dt} \quad (2.21.b)$$

$$\lambda_{ds} = L_s i_{ds} + L_m i_{dr} \quad (2.22.a)$$

$$\lambda_{qs} = L_s i_{qs} + L_m i_{qr} \quad (2.22.b)$$

$$\lambda_{dr} = L_r i_{dr} + L_m i_{ds} \quad (2.23.a)$$

$$\lambda_{qr} = L_r i_{qr} + L_m i_{ds} \quad (2.23.b)$$

where $L_s = L_{ls} + L_m$

$$L_r = L_{lr} + L_m$$

where ω_e is the rotational speed of the synchronous reference frame; $\omega_s = \omega_e - \omega_r$ is the slip frequency [69] and s is the slip; and ω_r is the electrical speed measured in [rad/s], which can be calculated by means of the pole numbers $\omega_r = \frac{p}{2}\omega_m$, where ω_m is the mechanical angular speed of the rotor.

Furthermore, $v_{ds}, v_{qs}, v_{dr}, v_{qr}, i_{ds}, i_{qs}, i_{dr}, i_{qr}, \lambda_{ds}, \lambda_{qs}, \lambda_{dr}, \lambda_{qr}$ are the (*d*-*q*) components of the stator and rotor in voltage, current and flux linkage, while R_r, R_s, L_s and L_r are the resistances of the rotor and the stator when L_m is the mutual inductance. The electromagnetic torque can be produced by the residual magnetism, which is stored in a form of magnetic field in the rotor and stator. This electromagnetic torque can be calculated by [70]:

$$T_e = \frac{3}{2} p(\lambda_{dr} i_{qs} - \lambda_{qr} i_{ds}) = \frac{3}{2} pL_m (i_{dr} i_{qs} - i_{qr} i_{ds}) \tag{2.24}$$

where p is the number of pole pairs and $L_M = \frac{3}{2} L_m$

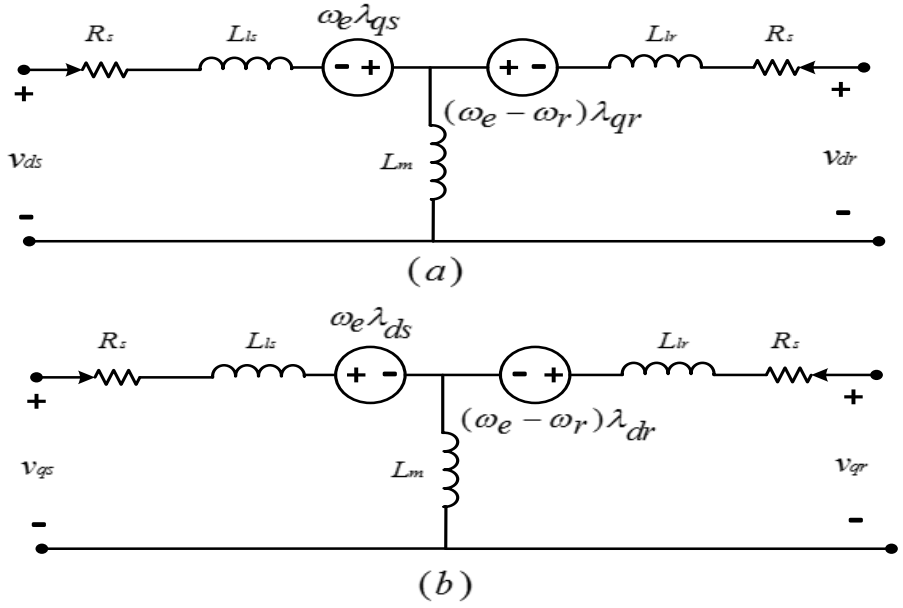

Figure 2.5: Equivalent circuit of the *d*-axis and *q*-axis in the arbitrary reference frame.

The power losses related to the rotor and stator resistance in the following model are neglected, and the power modeling for the active and reactive power of the DFIG can be written as follows [71]:

$$P_s = \frac{3}{2}(v_{ds} i_{ds} + v_{qs} i_{qs}) \tag{2.25}$$

$$Q_s = \frac{3}{2}(v_{qs} i_{ds} - v_{ds} i_{qs}) \tag{2.26}$$

$$P_r = \frac{3}{2}(v_{dr} i_{dr} + v_{qr} i_{qr}) \tag{2.27}$$

$$Q_r = \frac{3}{2}(v_{qr} i_{dr} - v_{dr} i_{qr}) \tag{2.28}$$

2.2.4 (α, β) Reference Frame

In order to describe the alpha-beta reference frame it must be considered that it resembles the *dq0* but it is stationary. Equations (2.20.a), (2.20.b) and (2.21.a), (2.21.b), taking into account the previous assumptions, are analyzed below.

Stator voltages and fluxes in the (α, β) reference frame:

$$v_{\alpha s} = R_s i_{\alpha s} + \frac{d}{dt}\lambda_{\alpha s} \tag{2.29.a}$$

$$v_{\beta s} = R_s i_{\beta s} + \frac{d}{dt}\lambda_{\beta s} \tag{2.29.b}$$

$$\lambda_{\alpha s} = \int \left(v_{\alpha s} - R_s i_{\alpha s}\right) \tag{2.30.a}$$

$$\lambda_{\beta s} = \int \left(v_{\beta s} - R_s i_{\beta s}\right) \tag{2.30.b}$$

The stator currents are:

$$i_{\alpha s} = \frac{L_{lr} + L_m}{L_{lr}L_{ls} + L_m(L_{lr} + L_{ls})}\lambda_{\alpha s} - \frac{L_m}{L_{lr}L_{ls} + L_m(L_{lr} + L_{ls})}\lambda_{\alpha r} \tag{2.31.a}$$

$$i_{\beta s} = \frac{L_{lr} + L_m}{L_{lr}L_{ls} + L_m(L_{lr} + L_{ls})}\lambda_{\beta s} - \frac{L_m}{L_{lr}L_{ls} + L_m(L_{lr} + L_{ls})}\lambda_{\beta r} \tag{2.31.b}$$

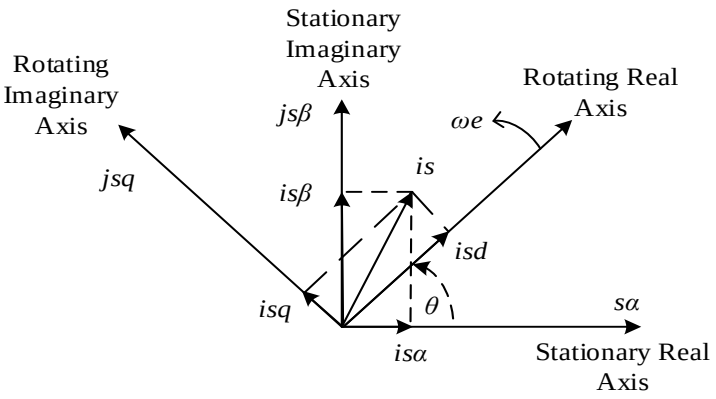

Figure 2.6: Relationship of current space vector components between (α, β) and (d, q) reference frames [84].

The equations of the α, β frame of the rotor's voltage and current are:

$$v_{\alpha r} = R_r i_{\alpha r} + \frac{d}{dt}\lambda_{\alpha r} + \omega_r \lambda_{\beta r} \tag{2.32.a}$$

$$v_{\beta r} = R_r i_{\beta r} + \frac{d}{dt}\lambda_{\beta r} - \omega_r \lambda_{\alpha r} \tag{2.32.b}$$

$$\lambda_{\alpha r} = \int \left(v_{\alpha r} - R_r i_{\alpha r} - \omega_r \lambda_{\beta r} \right) \tag{2.33.a}$$

$$\lambda_{\beta r} = \int \left(v_{\beta r} - R_r i_{\beta r} + \omega_r \lambda_{\alpha r} \right) \tag{2.33.b}$$

The α, β currents of the rotor are:

$$i_{\alpha r} = \frac{L_{lr} + L_m}{L_{lr}L_{ls} + L_m(L_{lr} + L_{ls})}\lambda_{\alpha r} - \frac{L_m}{L_{lr}L_{ls} + L_m(L_{lr} + L_{ls})}\lambda_{\alpha s} \tag{2.34.a}$$

$$i_{\beta r} = \frac{L_{lr} + L_m}{L_{lr}L_{ls} + L_m(L_{lr} + L_{ls})}\lambda_{\beta r} - \frac{L_m}{L_{lr}L_{ls} + L_m(L_{lr} + L_{ls})}\lambda_{\beta s} \tag{2.34.b}$$

The electromagnetic torque can be written as follows:

$$T_e = \frac{3}{2} p\left(\lambda_{\alpha r} i_{\beta r} - \lambda_{\beta r} i_{\alpha r} \right) \tag{2.35}$$

2.2.5 Conclusion

Induction generators are widely used in wind energy conversion systems. In this chapter, the advantages of using an induction generator instead of a synchronous generator were examined. As well, the dynamic modeling of induction machines was illustrated to explain the development of the subsequent machine control. Furthermore, algebraic equations describing the operation of a DFIG over two different reference frames were presented. The next chapter will focus on sliding mode controller applications to a doubly-fed induction generator.

Chapter 3

Sliding Mode Controller Application to DFIG

3.1. Introduction

Having the ability to manage systems in an uncertain context is one of the most intriguing desires of humans. This expectation can be reduced to a system theory context; indeed, the development of the control theory has given rise to several sophisticated control techniques devoted to solving the control problem for some classes of uncertain systems. Most of them are based on adaptation methods [72], relying both on identification and observation, and absolute stability methods [73, 74]. This reliance often leads to highly complex control algorithms whose implementation can imply a relevant computational cost and/or the use of very expensive devices. In recent years, an increasing interest in sliding modes has led to an almost complete formalization of the mathematical background and robustness properties in relation to system uncertainties and external disturbances of this control technique [75].

One way to deal with the uncertainty is variable structure systems (VSS), in which control can constrain the uncertain system behavior on an "a priori" specified manifold (the sliding manifold) by "brute force". In such systems, the control immediately reacts to any deviation of the system, steering it back to the constraint by means of a sufficiently energetic control effort. Any strictly satisfied equality removes one "uncertainty dimension".

In fact, VSS may be considered a general term for any dynamic system with discontinuous feedback control that can be defined by means of suitable sliding mode

techniques. Classical sliding mode control is based on the possibility of making and keeping an auxiliary output variable (i.e., the sliding variable) identically null. This then represents the deviation from the constraint by means of a discontinuous control acting on the first-time derivative of the sliding variable, and switching between high amplitude opposite values with theoretically infinite frequency. Moreover, due to its regularity properties and non-ideal realization, any system evolving in a boundary layer of the sliding manifold has the same trajectories (both system and control devices) as the ideal one, apart from some perturbing terms whose influence grows with the size of the boundary layer [76, 75]. Nevertheless, the implementation of sliding mode control techniques is troublesome because of the large control effort usually needed to ensure robustness properties, as well as the possibility that the so-called chattering phenomenon can arise [75].

The latter may lead to large undesired oscillations which can damage the controlled system. Recently-invented, higher-order sliding modes generalize the basic sliding mode idea. These are characterized by a discontinuous control acting on the higher-order time derivatives of the sliding variable instead of influencing its first-time derivative, as happens in standard sliding modes. Preserving the main advantages of the original approach with respect to robustness and ease of implementation, they entirely remove the chattering effect and guarantee even greater accuracy in the presence of plant and/or control device imperfections [77, 78]. The sliding order characterizes the smoothness degree of the system dynamics near the sliding mode.

The task in sliding mode control is to keep the system on the sliding manifold defined by the equality of the sliding variable to zero. The sliding order is defined as the number of continuous (and, of course, null within sliding mode) total time derivatives of

the sliding variable, zero included. Furthermore, an r-th-order real sliding mode provides sliding precision, i.e., the size of the boundary layer of the sliding manifold, up to the r-th-order with respect to plant imperfections, which result in delays in the switching [77, 78]. High-order sliding modes can appear naturally when fast dynamic actuators are used in VSS applications [78]. Indeed, when some types of dynamic actuators are present between a relay and the controlled process, the switching is moved to higher-order derivatives of the actual plant input. Thus, some new modes appear to be providing the exact satisfaction of the constraints and to be higher-order sliding modes. This phenomenon reveals itself by the spontaneous disappearance of chattering in VSS.

3.2. Second-order Sliding Modes

VSS dynamics is characterized by differential equations with a discontinuous right-hand side. As per the definition by Filippov, any discontinuous differential equation $\dot{X}=V(x)$, where $x \in IR^n$ and V is a locally bounded measurable vector function, is replaced by an equivalent differential inclusion, $\dot{X} \in V(x)$ [79]. In the simplest case, when v is continuous almost everywhere, $V(x)$ is the convex closure of the set of all possible limits of $v(z)$ *as* z --- x, while $\{z\}$ are continuity points of $v(z)$. Any solution of the differential equation is defined as an absolute continuous function $x(t)$ satisfying the differential inclusion almost everywhere.

The extension to the non-autonomous case is straightforward by considering time, t, as an element of vector, x. Consider an uncertain single-input nonlinear system whose dynamics is determined by the differential system:

$$\dot{X}(t) = f(x(t), t, u(t)) \qquad (3.1)$$

where x $\in$ X $\subset$ IR^n is the state vector, u $\in$ U $\subset$ IR is the bounded input, *t* is the independent variable time, and f: IR^{n+2} -----IR^n is a sufficiently smooth uncertain vector function. Assume that the control task is fulfilled by constraining the state trajectory on a proper sliding manifold in the state space defined by the vanishing of a corresponding sliding variable *s(t):* -

$$S(t) = S(x(t), t) = 0 \tag{3.2}$$

where s: IR^{n+1} ---- IR^n is a known single-valued function, such that its total time derivatives S^K , $K = 0, 1, \ldots, r - 1$ along the system trajectories exist and are single-valued functions of the system state *x*. The latter assumption means that discontinuity does not appear in the first $r - 1$ total time derivatives of the sliding variable *S*.

Definition l: Given the constraint function (3.2), its *r–th*-order sliding set is defined by the *r* equalities

$$S = S' = S'' = S^{(r-1)} = 0 \tag{3.3}$$

which constitute an *r*-dimensional condition on the system dynamics [80].

Definition 2: Let *r-th*-order sliding set (3.3) not be empty, and assume that it is locally an integral set in the Filippov sense, i.e., it consists of Filippov's trajectories of the discontinuous dynamic system. The corresponding motion of system (3.1) satisfying (3.3) is called an *r-th*-order sliding mode with respect to the constraint function, S. For shortening purposes, the words "r-*th-order sliding*" will be abridged below to "*r-sliding*".

Based on Definition 2, equation (3.1) evolves featuring a 2-sliding mode on the sliding manifold (3.2), if its state trajectories lie on the intersection of the two manifolds *S*

= 0 and $S' = 0$ in the state space. It is easy to see that, at 2-sliding points, Filippov's set of admissible velocities lies in the tangential space to $S = 0$ (Fig. l).

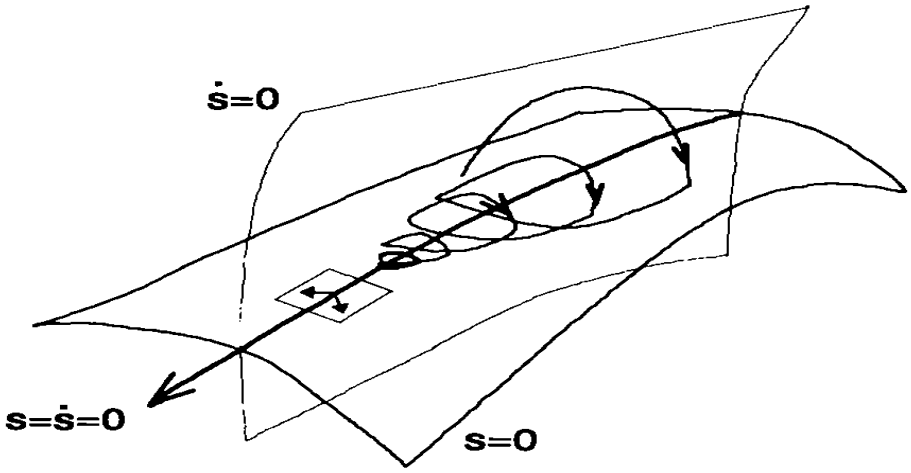

Figure 3.1: Second order sliding mode trajectory [80].

3.3. Sliding Variable Dynamics

Consider system (3.1) and assume that the control task is fulfilled by its zero dynamics [81] with respect to a properly defined output variable *S (x, t),* as in (3.2). By differentiating the sliding variable *s* twice, the following relationships are derived:

$$S'(\mathrm{t}) = S'(\mathrm{x(t)}, t, u(t)) = \frac{\partial}{\partial t} S(x, t) + \frac{\partial}{\partial x} S(x, t)\, f(x, t, u) \qquad (3.4)$$

$$S''(\mathrm{t}) = S''(\mathrm{x(t)}, t, u(t), u'(t)) = \frac{\partial}{\partial t} S'(x, t, u) + \frac{\partial}{\partial x} S'(x, t, u)\, f(x, t, u) + \frac{\partial}{\partial u} S'(x, ,t, u)\, u'(t) \qquad (3.5)$$

Depending on the relative degree [81] of the nonlinear second-order sliding mode (SISO) system (3.1), (3.2), different cases should be considered

a) Relative degree $P = 1$, i.e., $\frac{\partial}{\partial u} S' \neq 0$

As can be seen in (a), the classical approach to VSS by means of the first-order sliding mode control solves the control problem. However, the second-order sliding mode control can be used to avoid chattering as well. In fact, if the time derivative of the plant control, u'(t), is considered as the actual control variable, the 2-sliding mode control approach allows the definition of a discontinuous control u', steering both the sliding variable, *S*, and its time derivative, s', to zero, so that the plant control, u, is continuous and chattering is avoided [82, 83].

3.4. Chattering Avoidance

In some applications such as DC motors and aircraft, when the control is applied, it is important to avoid control chattering by providing continuous/smooth control signals. So, for instance, the aircraft aerodynamic surfaces cannot move back and forth with high frequency, it is desirable to retain the robustness/insensitivity of the control system to bounded model uncertainties and external disturbances.

When considering classical VSS, the control variable *u(t)* is a feedback-designed relay output. The most direct application of 2-sliding mode control is that of attaining the sliding motion on the sliding manifold (3.2) by means of a continuous bounded input *u(t).* This means that *u(t)* can be considered a continuous output of a suitable first-order dynamical system which can be driven by a proper discontinuous signal. Such first-order dynamics can be either inherent to the control device [77] or specially introduced for chattering elimination purposes [83], while the feedback control signal generated by the 2-sliding control algorithm is mostly the time-derivative of the plant input, *u(t).*

Consider system (3.1) and the constraint function (3.2). Assume that *F* and *S* are, respectively, C^1 and C^2 functions, and that the only available information consists of the

current values of t, $u(t)$, $S(x, t)$ and, possibly, of the sign of the time-derivative of the latter. The control goal for a 2-sliding mode controller is that of steering s to zero in finite time by means of a control, $u(t)$, that is continuously dependent on time.

To define the control problem, the following conditions must be assumed:

1) U = {u: $|u| < U_M$}, where $U_M > 1$ is a real constant; furthermore, the solution of (3.1) is well-defined for all t, if $u(t)$ is continuous and $u(t) \in U \; \forall t$.

2) There exists $u_1 \in (0, 1)$, such that for any continuous function $u(t)$ with $|u(t)| > u_1$, there is t_1, such that $S(t)u(t) > 0$ for each $t > t_1$. Hence, the control $u(t) = -sign\,[s\,(t_0)]$, where t_0 is the initial value of time, enables the hitting of the manifold (3.2) in finite time.

3) Let $S'(x, t, u)$ be the total time-derivative of the sliding variable $S(x, t)$, as defined in (3.4). There are positive constants t_0, $u_0 < 1$, Γ_m, Γ_M , such that if $|s(x, t)| < S_0$, then

$$\Gamma_m \leq \frac{\partial}{\partial u} S' \text{ (x, t, u)} \leq \Gamma_M, \;\; \forall u \in \text{U, x} \in \text{X} \tag{3.6}$$

and the inequality $|u| > u_0$ entails $Su' > O$.

4) There is a positive constant ϕ, such that within the region $|s| < S_0$, the following inequality holds: $\forall t, x \in X, u \in U$ [77].

$$\left| \frac{\partial}{\partial t} S'(x, t, u) + \frac{\partial}{\partial x} S'(x, t, u) f(x, t, u) \right| \leq \emptyset \tag{3.7}$$

Condition 2 means that, when starting from any point of the state space, it is possible to define a proper control, $u(t)$, steering the sliding variable within a set such that the boundedness conditions on the sliding dynamics defined by conditions 3 and 4 are satisfied. These conditions state that the second time-derivative of the sliding variable S,

evaluated with fixed values of the control u, is uniformly bounded in a bounded domain. It follows from the theorem on implicit function that there is a function u_{eq} *(t, x),* which can be viewed as Utkin's equivalent control [76], satisfying the equation $S' = 0$. Once s = 0 is achieved, the control $u = u_{eq}$ *(t, x)* would provide for the exact constraint fulfillment. Conditions 3 and 4 mean that $|s| < S_0$ implies $|u_{eq}| < u_0 < 1$, and that the velocity of the u_{eq} changing is bounded. This opens the possibility to approximate u_{eq} by a Lipschitzian control. Note that the unit upper bound for u_0 and u_1 can be considered as a scaling factor, and somewhere in the following it is not explicitly considered. Note also that linear dependence on control u is not required and that the usual form of the uncertain systems dealt with by the VSS theory, i.e., systems affine in the control, is a special case of the considered systems (3.1), (3.2).

3.5. Control Strategy of Doubly-fed Induction Generator by Applying SMC

Doubly-fed induction generator (GFIGs)-based wind turbine systems are one of the most popular machines in high power generation due to their many advantages. For instance, they can operate at different speeds, have independent regulation active and reactive power capability, have small power convertors, and can reduce power losses [83, 84]. However, regardless of the many positive aspects of GFIGs, challenges still remain in controlling the overall system for efficient and smooth operation. Oriented voltage stator or stator-flux-oriented vector control (VC) are used as a base in the conventional control of grid-connected DFIG wind turbine systems. In this control scheme, proportional-integral (PI) controllers are used to decouple the rotor current and regulate its components so that

the instantaneous stator active and reactive powers can be independently controlled through it.

The tracking performance is highly dependent on PI parameter tuning, such as stator and rotor resistances, inductances, and disturbances in the system. Consequently, there may be deteriorations in the performance as a result of the deviation of the actual machine parameters from the nominal values used in the control system, particularly when the PI controllers are operated under a fixed gain [85, 86].

In [87], an overview on the applications of DFIG in wind energy systems was presented. Several issues of control systems such as stand-alone operation, connection to balanced or unbalanced grids, sensorless control, and frequency support from DFIGs and low-voltage ride-through, were discussed. In [88], a machine inverter with three different controllers (PI, polynomial RST-based on pole placement theory and linear quadratic Gaussian approach with simulation validation) was used to regulate the stator active and reactive powers.

Nonlinear systems are normally subjected to uncertainties, parametric mismatches and external unknown disturbances. Thus, in order to carry out an effective control strategy for it, a sliding mode control (SMC) strategy is used. The SMC uses a switching term to keep the state on the manifold surface, and an additional compensation term can be used to deal with system modeling [89, 90]. Many different WECS configurations based on permanent magnet synchronous generator and DFGI have utilized the SMC strategy [91, 92]. It can be seen in [93] that without further discussion about the dc-link voltage regulations and its effect on the overall control system, a sliding surface which is based on the tracking error and its integration was used in the SMC approach in order to control only

the active-reactive power at the DFIG.

In [94], a similar approach to the SMC scheme was carried out for rotor-side control based on rotor speed tracking and grid-side control for dc-link voltage regulation. The proposed control scheme for both studies has thus far only been validated via a computer simulation. Additionally, the proposed SMC algorithms for the rotor- and grid-side power converters of a DFIG-based wind turbine under non-ideal grid voltage conditions have been verified by simulation in [95]. In [96], a second-order SMC scheme which employs an electromagnetic torque and d-component of the stator current, respectively, has been used in order to control the DFIG stator side active-reactive powers. In order to guarantee efficient power transfer via the back-to-back convertor, grid-side control and its effect on the proposed control system was excluded from this work. In [97], an approach similar to [96] was proposed, but with variable control gains. The control scheme was only verified by simulation due to the difficulties raised in the control design by the gains computation. In [98], the same second-order SMC was applied for the power control at the grid side of a DFIG-driven wind turbine. In order to establish the reference value for the extractable power based on the operation, a discrete second-order SMC scheme was used in [99] as an observer.

The main aim of this work is to develop an SMC scheme, where a switching term, an integral term and a compensating term can all be included to efficiently operate a DFIG-based WECS and deal with uncertainties, parametric mismatches and external disturbances and it is only the work which being validated by experimental system whereas the other works being only validate using simulation base. The control scheme will be used to ensure that the active-reactive power at the generator stator is regulated on a constant basis and to

maintain a continuous dc-link voltage at the back-to-back convertor.

The DFIG control includes controllers that function according to the rotor-side converter method (RSC) and the grid-side converter method (GSC). Hence, the active and reactive power controlled by RSC and DC-link voltage will be regulated by the GSC and also generate an independent reactive power that is injected into the grid [100].

3.5.1. Expressions of d and q Components at Stator and Rotor Sides to Calculate Power

$$\begin{cases} v_{sd} = R_s i_{sd} - \omega_s \varphi_{sq} + \dfrac{d\varphi_{sd}}{dt} \\ v_{sq} = R_s i_{sq} + \omega_s \varphi_{sq} + \dfrac{d\varphi_{sq}}{dt} \end{cases} \tag{3.8.a}$$

$$\begin{cases} v_{rd} = R_r i_{rd} - (\omega_s - \omega_r)\varphi_{rq} + \dfrac{d\varphi_{rd}}{dt} \\ v_{rq} = R_r i_{rq} + (\omega_s - \omega_r)\varphi_{rd} + \dfrac{d\varphi_{rq}}{dt} \end{cases} \tag{3.8b}$$

where v_{sd}, $v_{sq,}$ $i_{sd,}$ and i_{sq} are the *d-q* components of the stator voltage and current, φ_{sd} and φ_{sq} are the *d-q* components of the stator flux, R_s is the stator resistance, $v_{rd,}$ $v_{rq,}$ i_{rd} and i_{rq} are the *d-q* components of the rotor voltage and current, φ_{rd} and φ_{rq} are the *d-q* components of the rotor flux, R_r is the rotor resistance, ω_s is the synchronous angular speed, ω_r is the rotational speed and the slip angular speed can be expressed as $(\omega_s - \omega_r)$.

The stator and rotor fluxes can be expressed using stator and rotor currents:

$$\begin{cases} \varphi_{sd} = L_s i_{sd} + L_m i_{rd} \\ \varphi_{sq} = L_s i_{sq} + L_m i_{rq} \end{cases} \tag{3.9.a}$$

$$\begin{cases} \varphi_{rd} = L_r i_{rd} + L_m i_{sd} \\ \varphi_{rq} = L_r i_{rq} + L_m i_{sq} \end{cases} \tag{3.9.b}$$

where $L_{s,}$ L_r and L_m are the stator and the rotor inductance.

In the stator flux orientation, because of the q-axis alignment of the stator voltage with the reference frame, we can obtain [101], [102]:

$$\begin{cases} v_{sd} = 0 \\ v_{sq} = V_s \end{cases} \tag{3.10}$$

The stator flux can then be expressed as:

$$\begin{cases} \varphi_{sd} = \varphi_s \approx \dfrac{V_s}{\omega_s} \\ \varphi_{sq} \approx 0 \end{cases} \tag{3.11}$$

and the rotor current dynamics can be obtained by combining (3.8)– (3.11):

$$\begin{cases} \dfrac{di_{rd}}{dt} = -ai_{rd} + s\omega_s i_{rq} + \dfrac{R_s b}{\omega_s} V_s + \dfrac{1}{\sigma L_r} v_{rd} \\ \dfrac{di_{rq}}{dt} = -ai_{rq} - s\omega_s i_{rd} - bsV_s + \dfrac{1}{\sigma L_r} v_{rq} \end{cases} \tag{3.12}$$

where $\sigma = 1 - \dfrac{L_m^2}{L_s L_r}$ is the leakage factor, $s = \dfrac{\omega_s - \omega_r}{\omega_s}$ is the slip, $a = \dfrac{R_r L_s^2 + R_s L_m^2}{\sigma L_s^2 L_r}$, and $b = \dfrac{L_m}{\sigma L_s L_r}$. The power generated at the stator and rotor sides can be expressed as:

$$\begin{cases} P_s = \frac{3}{2}(v_{sd} i_{sd} + v_{sq} i_{sq}) \\ Q_s = \frac{3}{2}(v_{sq} i_{sd} - v_{sd} i_{sq}) \end{cases} \tag{3.13.a}$$

$$\begin{cases} P_r = \frac{3}{2}(v_{rd} i_{rd} + v_{rq} i_{rq}) \\ Q_r = \frac{3}{2}(v_{rq} i_{rd} - v_{rd} i_{rq}) \end{cases} \tag{3.13.b}$$

where P_s, Q_s, P_r and Q_r are the stator and rotor active and reactive powers, respectively. The powers can be expressed by substituting (3.8)– (3.11) in (3.13):

$$\begin{cases} P_s = -\frac{3}{2}\dfrac{L_m}{L_s} V_s i_{rq} \\ Q_s = \frac{3}{2}\left(\dfrac{V_s \varphi_s}{L_s} - \dfrac{L_m}{L_s} V_s i_{rd}\right) \end{cases} \tag{3.14.a}$$

$$\begin{cases} P_r = \frac{3}{2}\frac{L_m}{L_s} s V_s i_{qr} \\ Q_r = \frac{3}{2}\frac{L_m}{L_s} s V_s i_{dr} \end{cases} \quad (3.14.b)$$

From (3.14), the total powers can be obtained as:

$$\begin{cases} P_t = P_s + P_r = \frac{3}{2}(s-1)\frac{L_m}{L_s} V_s i_{rq} \\ Q_t = Q_s + Q_r = \frac{3}{2}(\frac{V_s \varphi_s}{L_s} + (s-1)\frac{L_m}{L_s} V_s i_{rd}) \end{cases} \quad (3.15)$$

where P_t and Q_t are the total active and reactive powers, respectively.

As can be seen in (3.15), the active and reactive powers can be controlled by the (*d*-*q*) components of the rotor current, such as:

$$\begin{bmatrix} P_t \\ Q_t \end{bmatrix} = \begin{bmatrix} 0 & \frac{3}{2}(s-1)\frac{L_m}{L_s} V_s \\ \frac{3}{2}(s-1)\frac{L_m}{L_s} V_s & 0 \end{bmatrix} \begin{bmatrix} i_{rd} \\ i_{rq} \end{bmatrix} + \begin{bmatrix} 0 \\ \frac{3}{2}\frac{V_s \varphi_s}{L_s} \end{bmatrix} \quad (3.16)$$

Therefore, tracking rotor currents will allow for the control of the total power, using (3.16).

3.5.2. DC-Link Modeling

The dc-link voltage dynamics can be expressed as:

$$C\frac{dV_{dc}}{dt} = I_g - I_r \quad (3.17)$$

where C is the dc-link capacitor, I_g is the grid current and the grid, and I_r is the rotor of the DFIG.

From (3.10), the active and reactive power can be calculated at the inverter output, as shown below:

$$P_g = \frac{3}{2} V_s i_{gq} \quad (3,18)$$

$$Q_g = -\frac{3}{2} V_s i_{gd} \quad (3.19)$$

The active power of the grid inverter can be calculated, assuming ideal inverter, as:

$$V_{\mathrm{dc}} I_g = \tfrac{3}{2} V_s i_{gq} \tag{3.20}$$

From (3.17) and (3.20), the dc-link voltage dynamics can be illustrated as:

$$\frac{dV_{\mathrm{dc}}}{dt} = \tfrac{3}{2}\frac{1}{C}\frac{V_s}{V_{\mathrm{dc}}} i_{gq} - \frac{1}{C} I_r \tag{3.21}$$

Meanwhile, the dynamics in (3.21) can be rearranged as:

$$\frac{dV_{\mathrm{dc}}}{dt} = \frac{1}{C} b_V i_{gq} + \frac{1}{C} \eta_V \tag{3.22}$$

where $b_V = \tfrac{3}{2}\dfrac{V_s}{V_{\mathrm{dc}}^*}$ with V_{dc}^* is the dc-link voltage and uncertainties can be calculated as $\eta_V = \Delta V_{\mathrm{dc}} - I_r$. Uncertainties occur due to variations between the actual voltage and the reference and the output current from the ac-dc converter [103].

3.5.3. Sliding Mode Control Design

3.5.3.1- Rotor-side Control

The control system is designed for active and reactive power by controlling the rotor currents (i_{rq}, i_{rd}). Therefore, to control the power, the rotor current should be regulated. The references of the rotor current can be tracked and obtained from (3.16), such as:

$$\begin{bmatrix} i_{rd}^* \\ i_{rq}^* \end{bmatrix} = \begin{bmatrix} 0 & \tfrac{3}{2}(s-1)\dfrac{L_m}{L_s} V_s \\ \tfrac{3}{2}(s-1)\dfrac{L_m}{L_s} V_s & 0 \end{bmatrix}^{-1} \left\{ \begin{bmatrix} P_t^* \\ Q_t^* \end{bmatrix} - \begin{bmatrix} 0 \\ \tfrac{3}{2}\dfrac{V_s \varphi_s}{L_s} \end{bmatrix} \right\} \tag{3.23}$$

where i_{rd}^* and i_{rq}^* are the references of the rotor current components (d, q), and P_t^* and Q_t^* are the references for the active power and reactive power, respectively.

The system uncertainties have been added up to rotor current dynamics (3.12) in order to be used in the current control design, as follows:

$$\begin{cases} \dfrac{di_{rd}}{dt} = -ai_{rd} + s\omega_s i_{rq} + \dfrac{R_s b}{\omega_s} V_s + \dfrac{1}{\sigma L_r} v_{rd} + \dfrac{1}{\sigma L_r} \eta_d \\ \dfrac{di_{rq}}{dt} = -ai_{rq} - s\omega_s i_{rd} - bsV_s + \dfrac{1}{\sigma L_r} v_{rq} + \dfrac{1}{\sigma L_r} \eta_q \end{cases} \tag{3.24}$$

where η_d and η_q are the uncertainties of the rotor current components (d, q), which are considered unknown. The uncertainties include parametric variations, unmodeled quantities, and any external disturbances.

Here, (3.24) has been used to track the error dynamics of the *d*-component of the rotor current:

$$\begin{aligned} \dot{e}_d(t) &= \dot{i}_{rd}^* - \dot{i}_{rd} \\ &= \dot{i}_{rd}^* - \left(-ai_{rd} + s\omega_s i_{rq} + \frac{R_s b}{\omega_s} V_s + \frac{1}{\sigma L_r} v_{rd} \right) - \frac{1}{\sigma L_r} \eta_d \\ &= u_d - \frac{1}{\sigma L_r} \eta_d \end{aligned} \tag{3.25}$$

where $e_d = i_{rd}^* - i_{rd}$ is the tracking error for the *d*-component of the rotor current. The SMC law for the d-component is given by:

$$\begin{cases} u_d(t) = -k_{d1} \operatorname{sgn}(e_d(t)) - x_d(t) \\ \dot{x}_d(t) = k_{d2} e_d(t) + k_{d3} \operatorname{sgn}(e_d(t)) \end{cases} \tag{3.26}$$

From (3.25) and (3.26), the control input v_{rd}^* can be formulated as:

$$\begin{cases} v_{rd}^* = \sigma L_r \left(\dot{i}_{rd}^* + ai_{rd} - s\omega_s i_{rq} - \dfrac{R_s b}{\omega_s} V_s + k_{d1} \operatorname{sgn}(e_d) + x_d \right) \\ \dot{x}_d = k_{d2} e_d + k_{d3} \operatorname{sgn}(e_d) \end{cases} \tag{3.27}$$

The design of the SMC law (3.27) includes switching, compensating, and integral terms in order to overcome the issues of nonlinear dynamics and uncertainties in the system. it is only the work which being validated by experimental system whereas the other works

being only validate using simulation base. At the same time, (3.24) has been used to track the error dynamics of the *d*-component of the rotor current:

$$\begin{aligned}\dot{e}_q(t) &= \dot{i}_{rq}^{*} - \dot{i}_{rq} \\ &= \dot{i}_{rq}^{*} - \left(-ai_{rq} - s\omega_s i_{rd} - bsV_s + \frac{1}{\sigma L_r} v_{rq} \right) - \frac{1}{\sigma L_r}\eta_q \\ &= u_q - \frac{1}{\sigma L_r}\eta_q\end{aligned} \tag{3.28}$$

where $e_q = i_{rq}^{*} - i_{rq}$ is the tracking error of the rotor current component (q).

Similar to (3.26), the SMC law is proposed as:

$$\begin{cases} u_q(t) = -k_{q1}\,\mathrm{sgn}(e_q(t)) - x_q(t) \\ \dot{x}_q(t) = k_{q2}e_q(t) + k_{q3}\,\mathrm{sgn}(e_q(t)) \end{cases} \tag{3.29}$$

From (3.28) and (3.29), the control input v_{rq}^{*} can be expressed as:

$$\begin{cases} v_{rq}^{*} = \sigma L_r \left(\dot{i}_{rq}^{*} + ai_{rq} + s\omega_s i_{rd} + bsV_s + k_{q1}\,\mathrm{sgn}(e_q) + x_q \right) \\ \dot{x}_q = k_{q2}e_q + k_{q3}\,\mathrm{sgn}(e_q) \end{cases} \tag{3.30}$$

3.5.3.2- Grid-side Control

The main purpose of using a grid-side controller is to maintain constant dc-link voltage which is not insensitive to the rotor power flow [104]. To achieve this objective, a sliding mode controller control strategy with a reference frame aligned with the stator voltage position is used. This allows independent control of the dc-link voltage and the reactive power between the converter and the grid.

The machine side needs a dc power supply. The required dc voltage is generated by using another source of voltage, which is connected to the stator terminals of the generator through an ac grid. In order to keep the dc link voltage constant, a PWM and capacitor are used to eliminate the ripples and maintain smooth dc voltage.

The dc-link voltage error is given by:

$$\begin{aligned}\dot{e}_V &= \dot{V}_{\mathrm{dc}}^{*} - \dot{V}_{\mathrm{dc}} \\ &= \dot{V}_{\mathrm{dc}}^{*} - \frac{1}{C} b_V i_{gq} - \frac{1}{C}\eta_V \\ &= u_V - \frac{1}{C}\eta_V\end{aligned} \tag{3.31}$$

where u_V is the new control input.

Similarly, in the generator control side, the proposed SMC (3.26) is used:

$$\begin{cases} u_V(t) = -k_{V1}\,\mathrm{sgn}(e_V(t)) - x_V(t) \\ \dot{x}_V(t) = k_{V2} e_V(t) + k_{V3}\,\mathrm{sgn}(e_V(t)) \end{cases} \tag{3.32}$$

From (3.31) and (3.32), the control input i_{gq}^{*} is given by:

$$\begin{cases} i_{gq}^{*} = \dfrac{C}{b_V}\left(\dot{V}_{\mathrm{dc}}^{*} + k_{V1}\,\mathrm{sgn}(e_V) + x_V\right) \\ \dot{x}_V = k_{V2} e_V + k_{V3}\,\mathrm{sgn}(e_V) \end{cases} \tag{3.33}$$

The grid-side control system consists of the dc-link voltage controller (based on the SMC method) as the outer loop control, which provides the reference for the grid current controller as the inner-loop controller. The conventional vector control (VC) scheme is omitted in this section, as it does not contribute to this work. However, details can be found in [105].

The overall control scheme for active-reactive power at the rotor side and dc-link voltage at the back-to-back converter can be seen in Fig. 3.2.

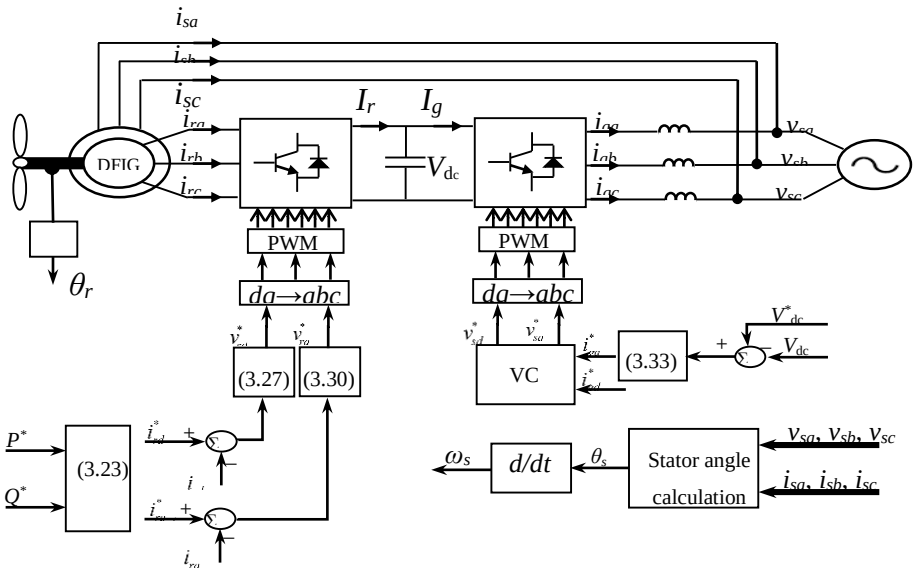

Fig. 3.2: Proposed SMC for DFIG-based wind energy conversion system.

3.5.3 Conclusion

In this chapter, a detailed wind turbine control system was presented. Two controllers were proposed to control the power generated by the DFIG on both sides (i.e., rotor and grid sides) using a sliding mode controller. The SMC scheme was also developed, where a switching strategy for the converter, an integral and a compensating terms were included to optimize the operation of the DFIG-based WECS and deals with uncertainties, parametric mismatches and external disturbances.

Chapter 4

Experimentation and Experiment Results

4.1 Hardware Components

The experimental system shown in Fig. 4.2 consists of a 4-pole three-phase wound-rotor induction machine, while Fig. 4.1 shows a schematic of the connected experiment setup to emulate WECS. Each phase of the stator winding is accessible via the connection module to allow wye or delta connections. The rotor is wye connected to four slip rings to give access to all windings, including neutral. The phases, in brief, are described as follows: 1) a four quadrant dynamometer-type of squirrel cage induction motor with an encoder feedback; 2) two back-to-back 6-pulse IGBT inverters, the switching frequency (here, 3kHz) for which should be chosen in such a way that the balance between switching losses and accuracy of the desired signals is achieved; and 3) a line inductor with a 2 kW variable power supply, an Opal RT data acquisition system OP8600, and a real-time digital simulator OP5600, which is a powerful tool for rapid control prototyping with a processor Intel Xeon Quad Core 2.4 GHz.

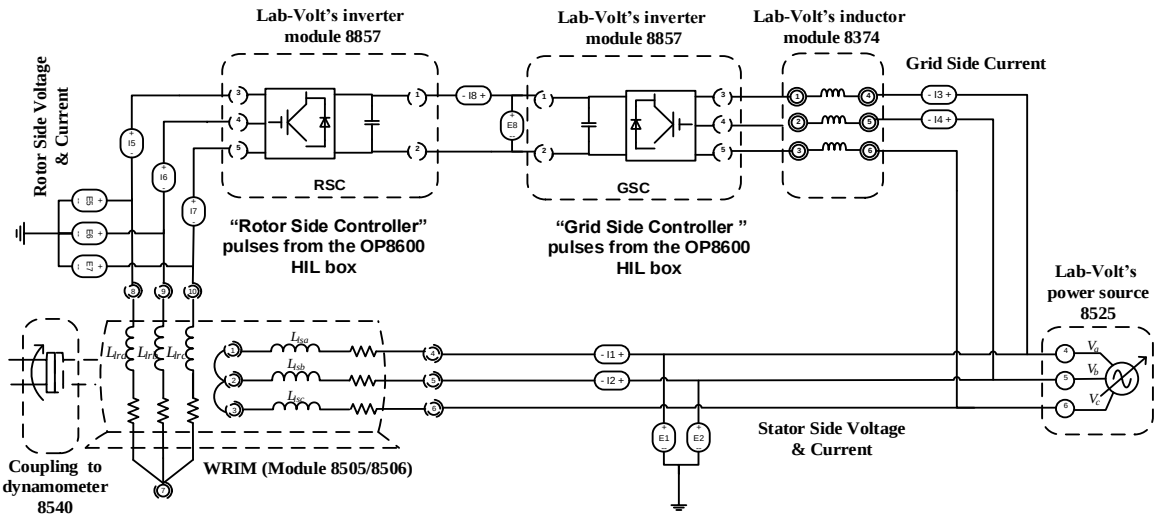

4.1: Schematic of the connected experiment setup to emulate WECS.

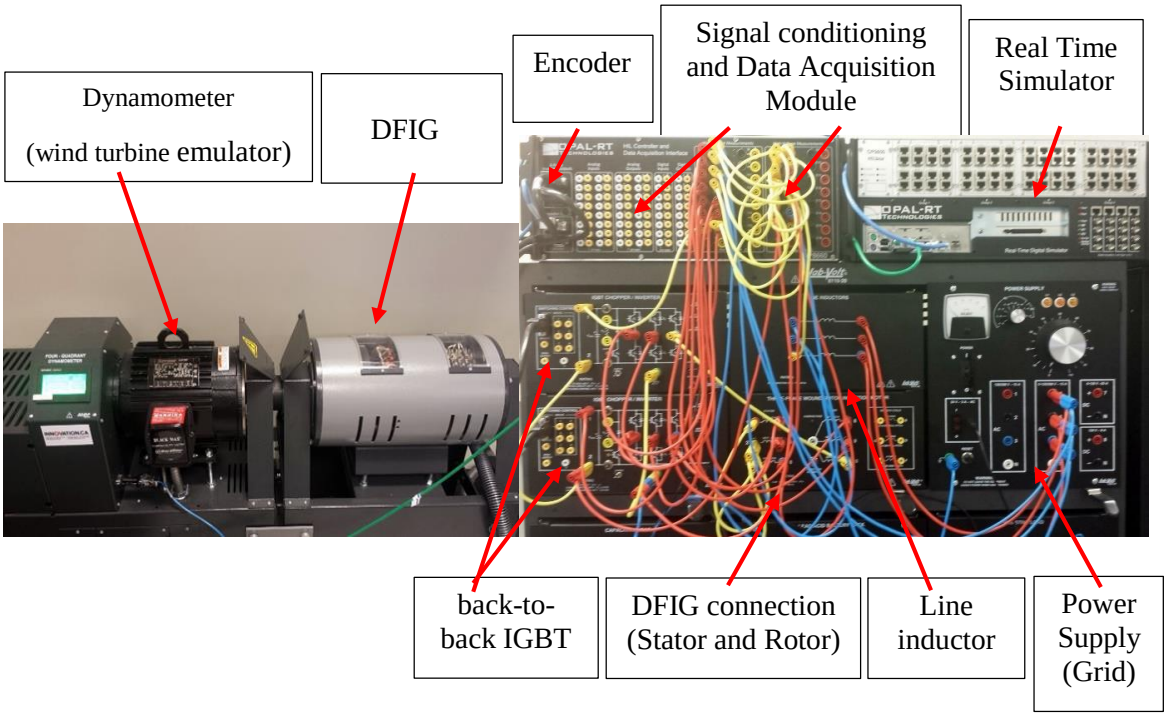

Figure 4.2: Experimental setup to emulate WECS.

4.1.2 Real-time Simulation Environment

Real-time simulation (RTS) technology can be defined as a computer model building from a real physical system that can be run in the computer at the same rate as

actual time [80]. Therefore, the RTS has brought many advantages to engineers, such as cost avoidance, increased quality, complete physical testing, reuse of simulator, more tests in the lab, early fault detection, increased productivity, and fewer onsite tests. Real-time system configurations can be classified into three application categories, as shown in Fig. (4.3) [106], [107].

i- Rapid control prototyping (RCP)

ii- Hardware-in-the-loop (HIL)

iii- Pure Simulation (PS)

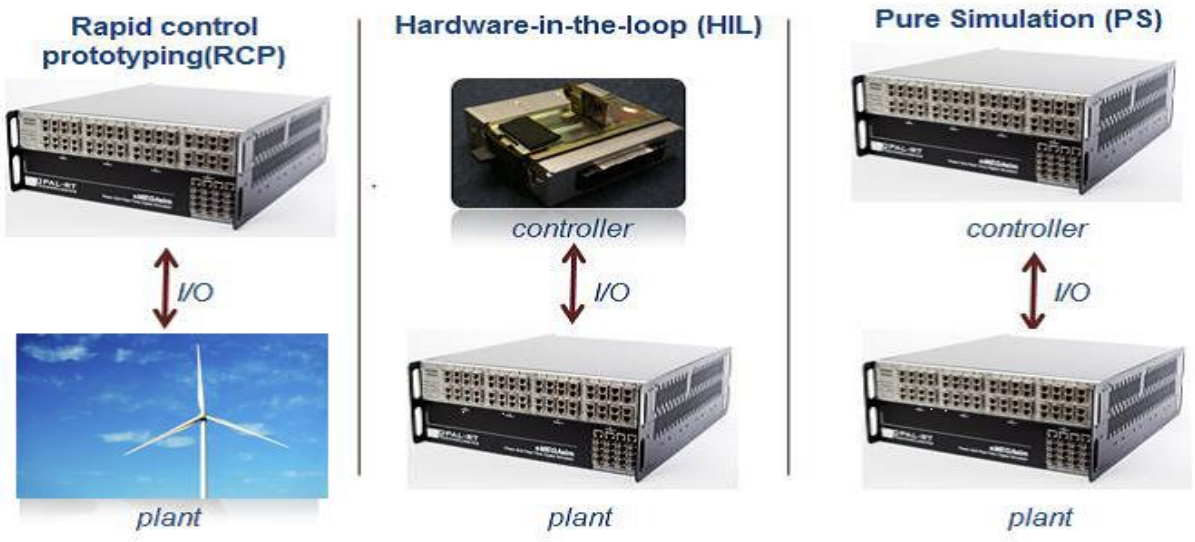

Figure 4.3: Applications categories of real-time system configurations [106] [107].

In RCP applications, a real-time simulator is used to implement a controller for plant model and connect to a physical system via input and output of the simulator ports. This application category provides numerous advantages, including faster implementation, greater flexibility, and ease of debugging [82]. In contrast, HIL is used to test real controllers connected to a simulated plant model. The simulated plant model usually costs

less and is more stable than a real plant. In addition to the advantages mentioned above, HIL allows for model testing at reduced cost and without risk. In PS applications, a real-time simulator is used to implement both the controller model and a virtual plant model, as illustrated in Fig. (4.3) [106] [107].

4.1.3 RT-LAB™ Overview

The software used in this study is RT-LAB™ (Workbench) Version: v10.5.7.334. RT-LAB is a distributed real-time platform that enables engineers and researchers to run Simulink dynamic models in real-time with hardware-in-the-loop (HIL), at low cost with high accuracy and within a very short time. Its scalability allows the developer to add computing power where and when it is needed. It is flexible to complex simulation and control problems, whether a real-time HIL application or speeding up a model execution, control and test. The embedded device in a real-time system is given a predetermined amount of time (1, 5, or 20 min) to read input signals (e.g., sensors), to perform all necessary calculations (e.g., control algorithms), and to write all outputs (e.g., analog/digital outputs). The model is solved by fixed-step solvers within fixed intervals called step size, as shown in Fig. (4.4).

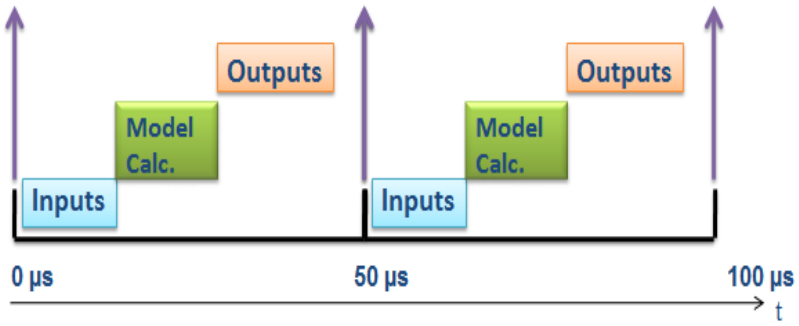

Figure 4.4: Proper choices for time step simulations [108].

As shown in Fig. (4.5), overrun occurs when a predetermined time step is too short and cannot perform the process of the simulation. To overcome overrun, the time step should be increased to omit this interference by the next interval. However, increasing the time step decreases the accuracy of the results [108].

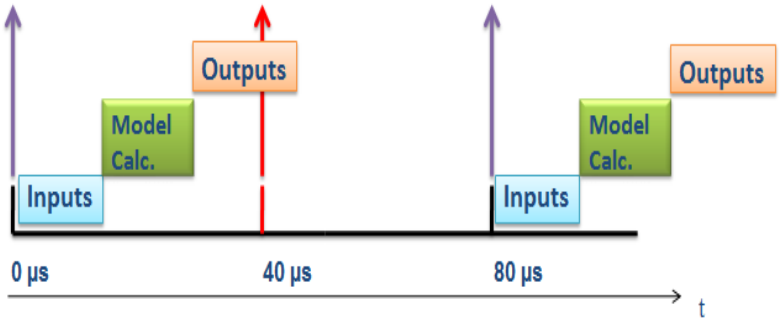

Figure 4.5: Improper choice for time step simulation [108]

4.1.4. Hardware Details

The simulator utilized in this study is an OP5600 real-time digital simulator. This kind of simulator is used to demonstrate the real-time performance of the active and reactive power control of a DFIG-based wind energy conversion system. The OP5600 is built using the OP8660 HIL controller and data acquisition interface, which is designed to extend the capabilities of the OP5600 real-time digital simulator by providing multiple I/O channels specifically tailored for power electronics and power systems applications. The OP8660 simplifies the connectivity between a virtual environment (real-time simulator) and real experimental systems by providing a secure, robust and easy-to-use interface that is ideal for training and educational environments.

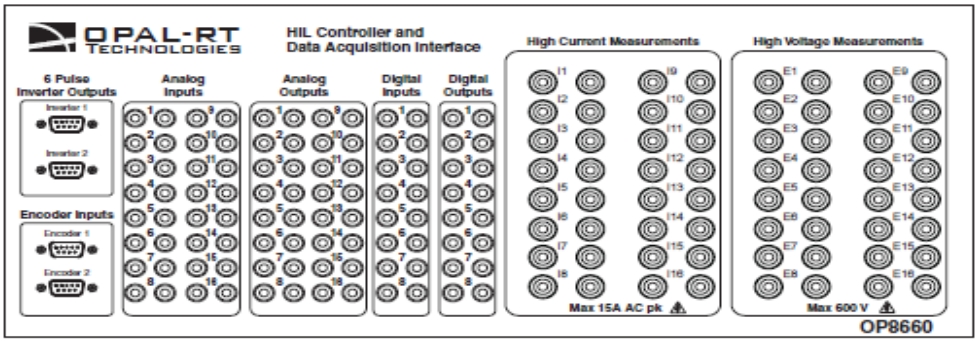

Figure 4.6: *OP8660* HIL controller and data acquisition interface [109].

The RCP-EC2K kit contains a powerful real-time target computer-equipped 12 to 3.3 GHz processor cores running Red Hat Linux real-time operating and two user-programmable FPGA-based I/O management options, powered by the Xilinx Spartan-3 or more powerful Virtex-6 FPGA processor. Available expansion slots accommodate up to 8 signal conditioning and analog /digital converters modules with 16 or 32 channels each, for a total of fast 128 analogs or 256 discrete, or a mix of analog and digital signals [109]. It releases as a single target that can be networked into a multiple-target *PC* cluster or for complex applications capable of implementing large models with more than 3000 *I/O* channels and a time step below 25 micros. This also allows including HIL testing, as shown in Fig. (4.6). Complex power grids, micro-grids, wind farms, hybrid vehicles, electrical aircraft, electrical ships and power electronic systems can be simulated with a time step as low as 10 microseconds (or less than 250 nanoseconds for some subsystems) in order to increase accuracy. In addition, it offers versatile monitoring on the front panel through RJ45 to mini-BNC connectors [109]. The front and back views of the OP5600 real-time digital simulator are depicted in Fig. (4.7).

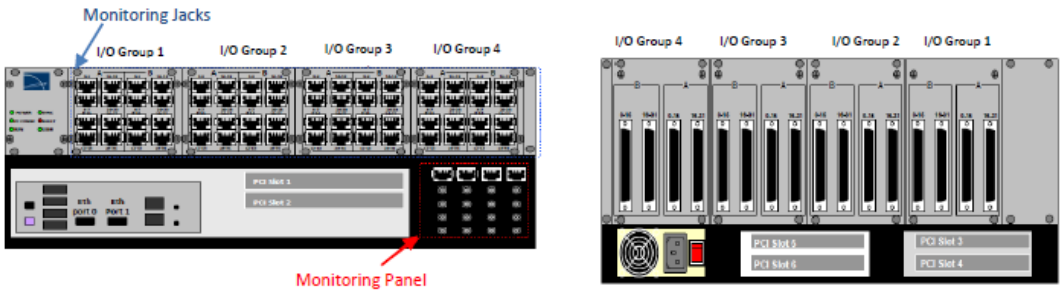

(a) Front view (b) Back view

Figure 4.7: *OP5600* real-time simulation target view [109].

5.1.5. Model Building & Execution in RT-LAB™ for Real-Time Simulation

The RT-LAB™ is built from Simulink model which has a rapid controller prototyping (RCP) for real life simulation and control of a grid connected doubly fed induction generator (DFIG) based laboratory size wind turbine emulator for wind energy conversation system. To define models and corresponding parameters in the RT-LAB™, Simulink is used to accomplish that with real-time multi-processing system. DFIG based wind turbine (DFIG-WT) Simulink model is applied in RT-LAB™ setting by carrying out the following steps.

- Regrouping into subsystems
- Adding the OpComm block(s)
- Maximizing parallel execution and state variables
- Setting the real-time parameters

Two separated subsystems are used when applying the model to different target processors or nodes. They are as the following

1. Console subsystem, which has to be identified by the prefix (SC_) by its name. this subsystem is carried out in the PC command station which

includes user interface blocks such as displays, scopes, and reference command.

2. Master subsystem, which also has to be identified by the prefix (SM_) by its name. this subsystem is performed in the CPU core processor of the OP5600 which contains all the computational elements of the model, the mathematical operations of the algorithms and the input-output blocks. RT-LAB^{TM} OpComm as shown in figure 4.8 are used to communicate and synchronize between the two subsystems because they are applied to different targets or nodes.

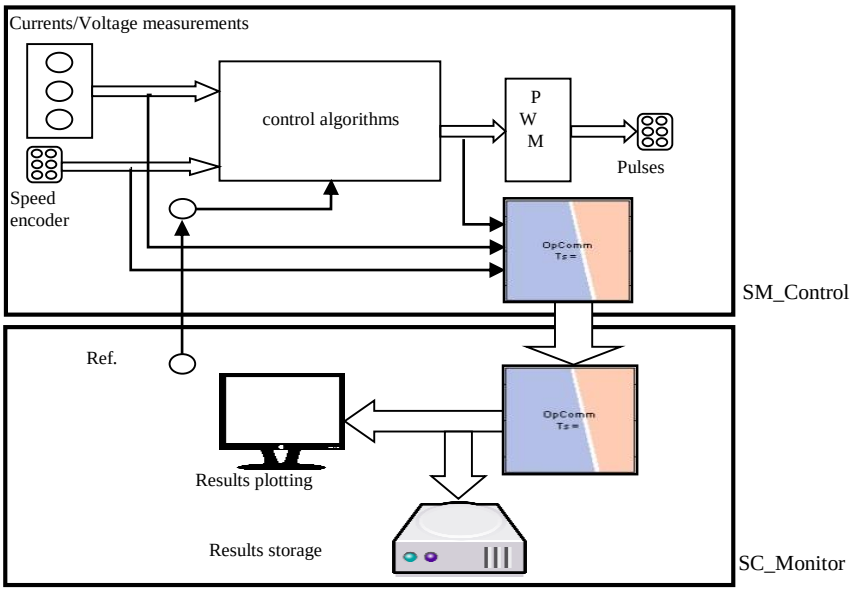

Figure 4.8: Subsystems of the model in RT-LAB.

The RT-LAB^{TM} is used to open the Simulink model of the control system and then the real-time target (OP5600) is being compiled. After that, it is loaded automatically by RT-LAB^{TM} into the CPU core of the OP5600 for the master subsystem. A real-time OP5600 digital simulator, contains analog and digital I/O signal modules, a multi-core

processor and FPGA that runs RT-LAB^{TM} real-time simulation platform. The OP8660, HIL Controller and Data Acquisition Interface, is a signal conditioning interface simplifies the connectivity between the virtual environment (the real-time simulator OP5600) and the real experimental system (Dynamometer, DFIG, power electronics inverters, grid, load) as shown in Figure 4.9

Finally, the subsystems of the model are simultaneously implemented in the CPU core of the OP5600. Furthermore, the wind energy conversion system in real time for the SC subsystem is run by the SM subsystem, and the command host-PC where the RT-LAB^{TM} is used to manage all the communication, sequencing and the synchronization.

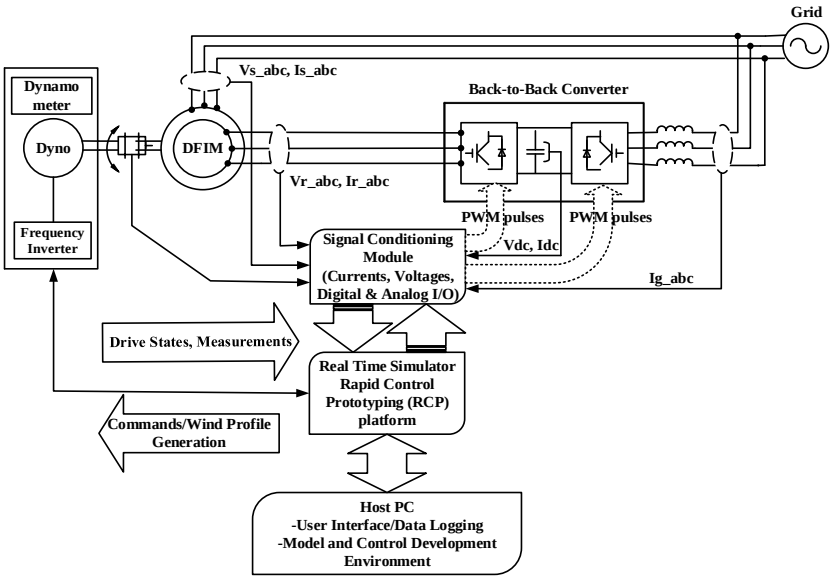

Figure 4.9: Execution of DFIG-based wind energy conversion system in real-time simulation.

4.2. Results and Discussion

Figure 4.10 illustrates the experimental DFIG-based WECS. As can be seen from the figure, this experiment consisted of a 2kW DFIG generator attached to a dynamometer that can be run at different speeds, so that a wind turbine, back-to-back converters, an inductive filter, and a three-phase power supply can be emulated to the grid. More details

about the properties of the elements can be found in Table I in the Appendix. Furthermore, a data acquisition interface (OP8660) was used to measure the voltages and currents. The Math-lab Simulink® was used to develop the SMC system, which then was run in the OPAL-RT real-time simulator (OP5600) via the software RT-LAB® [109].

Table II in the Appendix shows the parameters, which were kept constant throughout the experiment. In this control scheme, the proposed control system SMC was used to control the rotor currents (i_{rd}, i_{rq}) directly, while the powers (P_t, Q_t) were controlled by the rotor currents indirectly through the reference model (3.23). Thus, only the results obtained for rotor currents were discussed, as they were the quantities most affected by the control system.

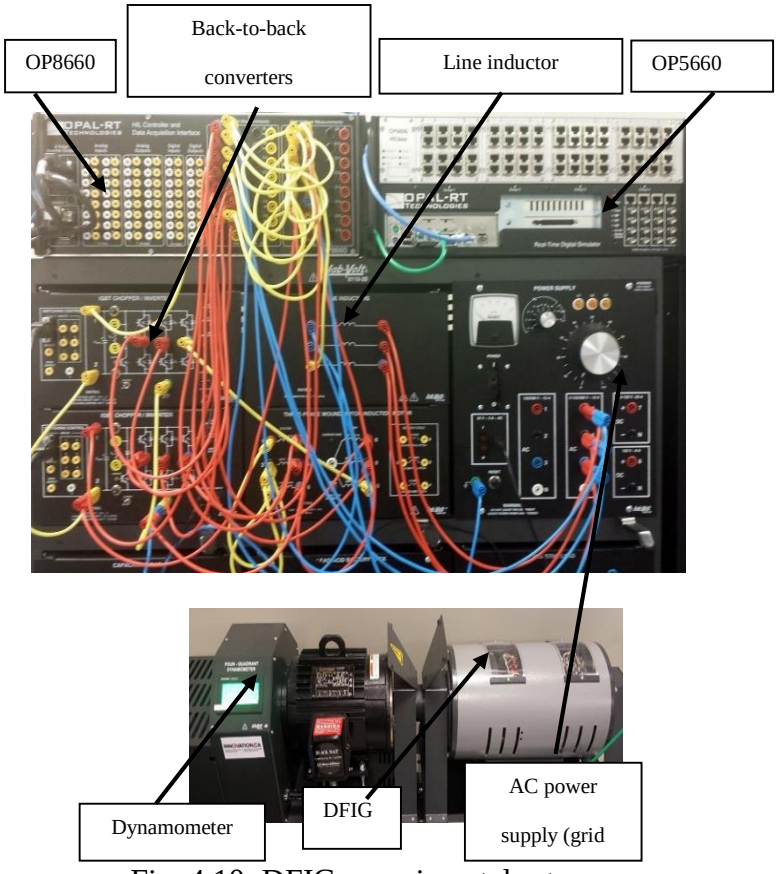

Fig. 4.10: DFIG experimental setup

4.2.1. Operation Under Constant Rotor Speed, Constant dc-link Voltage, and Variable Rotor Currents.

To start with, under a constant rotor speed (1800 rpm), which is a constant reference for the dc-link voltage and variable profiles for the *d-q* components of the rotor current, the proposed SMC system for operating the DFIG-based WECS was tested. Figure 4.11a illustrates the currents' responses that were determined in the experiment. It can be observed from these responses that the tracking was successfully achieved with good performance in terms of transient regime, overshoot, settling, and rise time. Moreover, as shown in Fig. 4.11b, it succeeded in regulating the dc-link voltage to be constant:

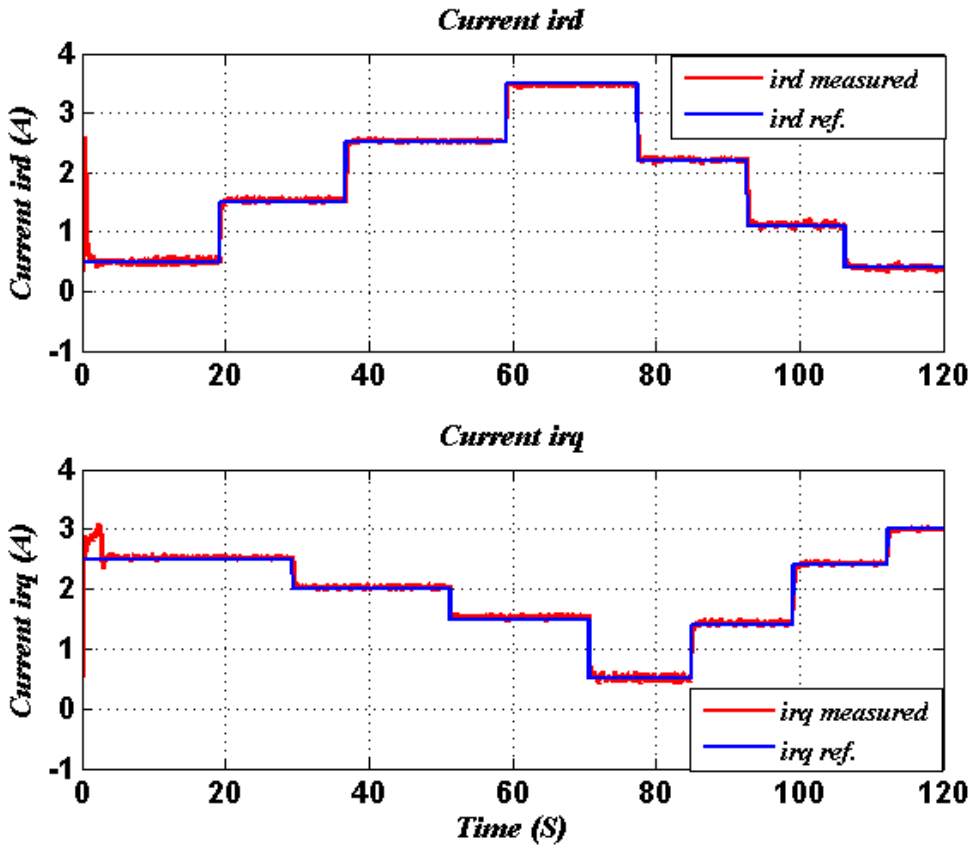

Fig. 4.11a: Rotor current *d-q* responses

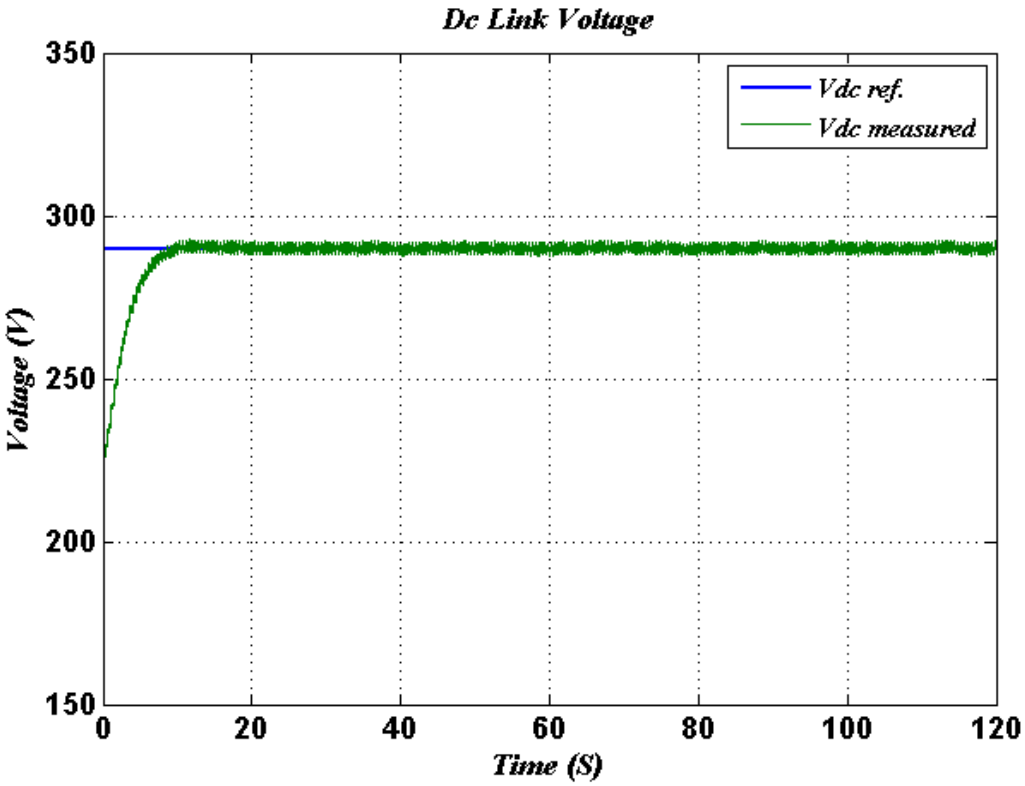

Fig. 4.11b: dc-link voltage responses.

4.2.2. Operation Under Constant Rotor Speed, Variable dc-link Voltage, and Variable Rotor Currents

Two steps were carried out before the SMC voltage controller (3.33) was tested under variable voltage profile:

1- Both the rotor speed and currents were kept constant.

2- The voltage reference was increased and decreased at different step levels.

In Fig. 4.12a, we can see that rotor current regulation, despite variations in dc-link voltage, has followed the constant reference shown in Fig. 4.12b. Furthermore, it can also be observed that voltage tracking occurred with good performance in terms of transient regime, overshoot, settling, and rise time. However, in real applications, the dc-link voltage

has to be maintained constantly. This experiment has shown that the proposed SMC system has the capability of operating under different voltage levels.

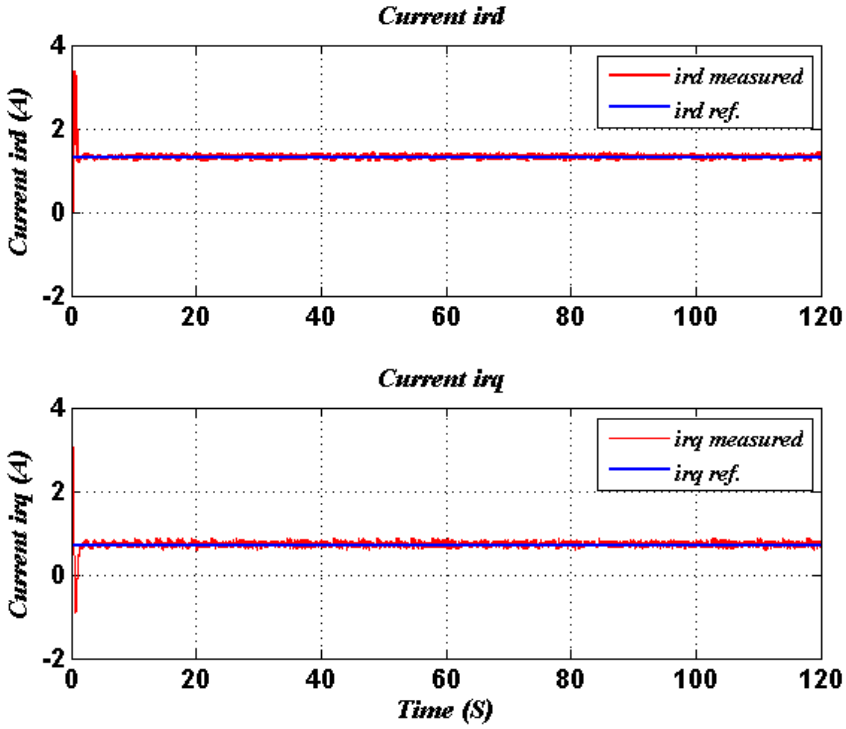

Fig. 4.12a: Rotor current *d-q* responses

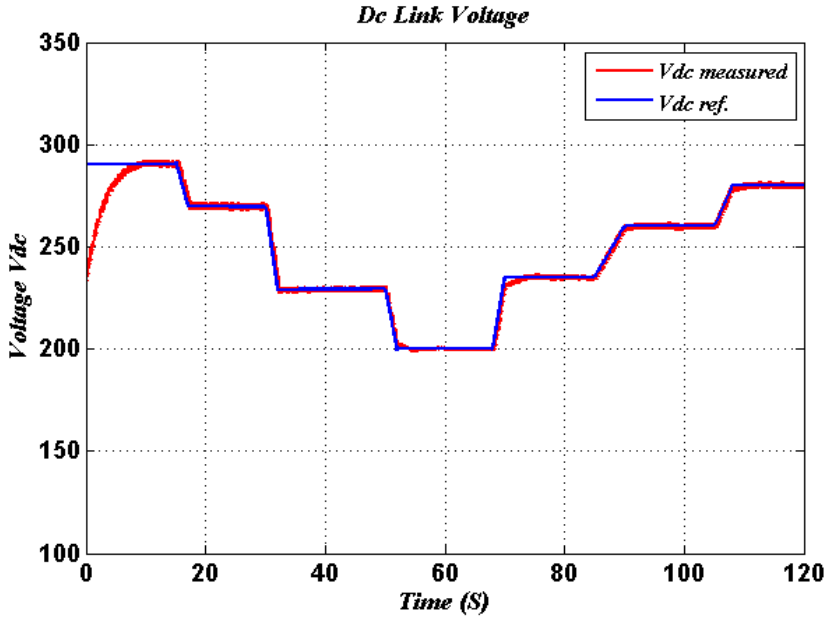

Fig. 4.12b: dc-link voltage responses.

4.2.3. Operation Under Variable Rotor Speed, Constant dc-link Voltage, and Rotor Currents

For this part of the experiment, it can be seen in Fig. 6a that the rotor speed was varied with an up-down profile to enable emulation of wind turbine operation under variable wind speeds. This was carried out so that the quantities (dc-link voltage and *d-q* rotor current) could be maintained at a constant, regardless of any variations in rotor speed. Furthermore, as can be seen in Figs. 4.13a and 4.13b, the objective was successfully realized with a good performance at the rotor speed transitions. Figure 4.14 shows the d-q rotor current results that were taken from (3.11), where a conventional vector control scheme based on proportional-integral (PI) regulators was used. The q-current was affected by the rotor speed transition, as indicated by the appearance of picks at each transition, and thus was almost eliminated by the proposed SMC system. According to the obtained results, the proposed system was more advantageous over traditional methods.

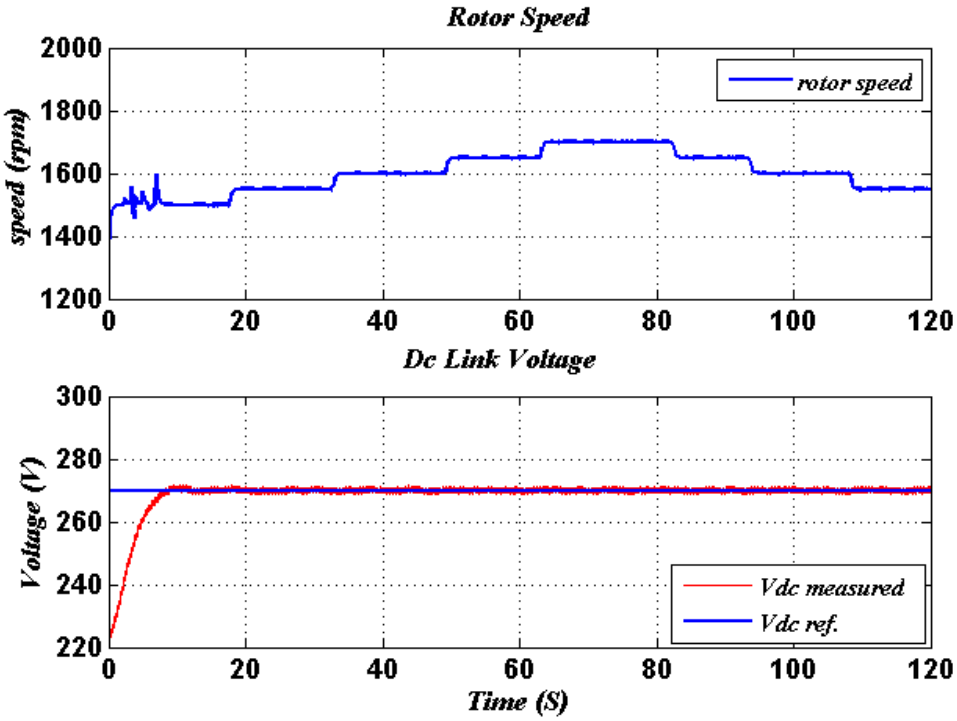

Fig 4.13 a: Dc-link response to rotor speed profile changing

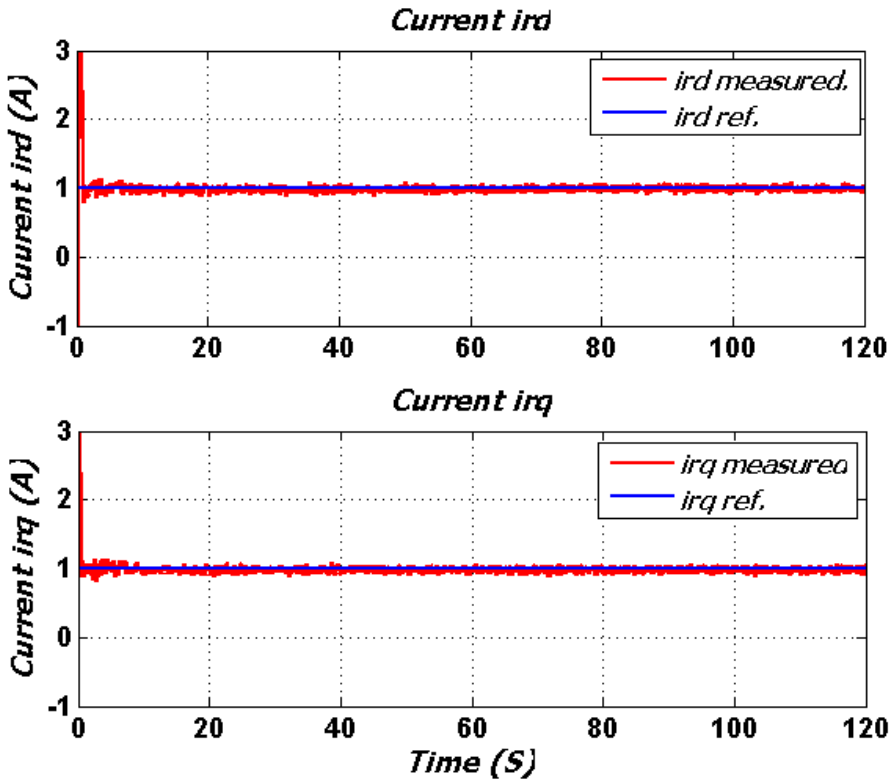

Fig. 4.13b: Rotor current, *d-q* response to rotor speed profile changing

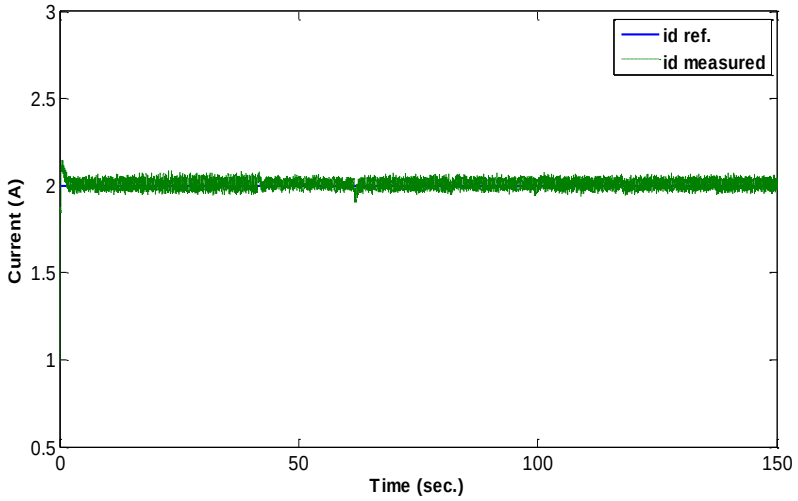

Fig 4.14 a : : Rotor current response *d* using the conventional control scheme [85]

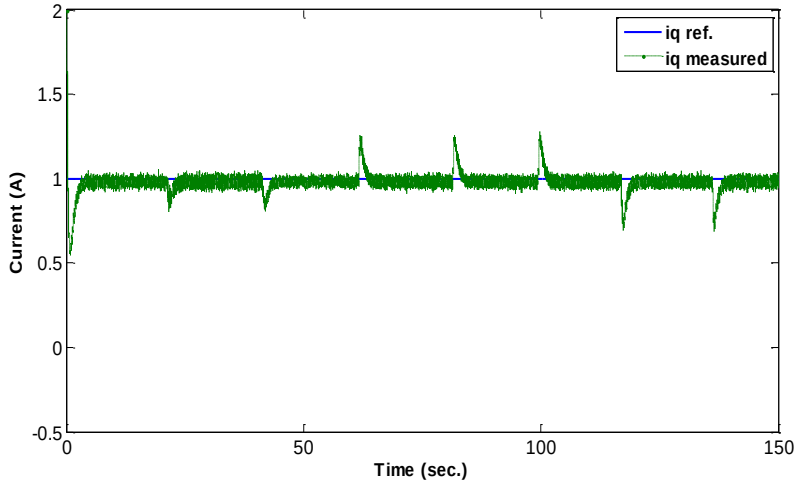

Fig.4.14b: Rotor current response *q* using the conventional control scheme [85]

4.2.4 Robustness to Parametric Mismatches

The values of the parameters in the control implementation were changed prior to verifying the robustness of the proposed SMC system to parametric mismatches. The changes were as follows:

1- 50% increase in rotor resistance (R_r)

2- 20% reduction in rotor inductance (L_r)

The objective for doing this was to keep all quantities (dc-link voltage and *d-q* rotor current) constant even with variations in rotor speed and using parameters in the control implementation. Figure 4.15 indicates the results obtained for the voltage and d-q current tracking. As can be seen, the regulation was successfully achieved, regardless of the inaccuracies in the parameters of the control law. This verifies the robustness of the proposed SMC system.

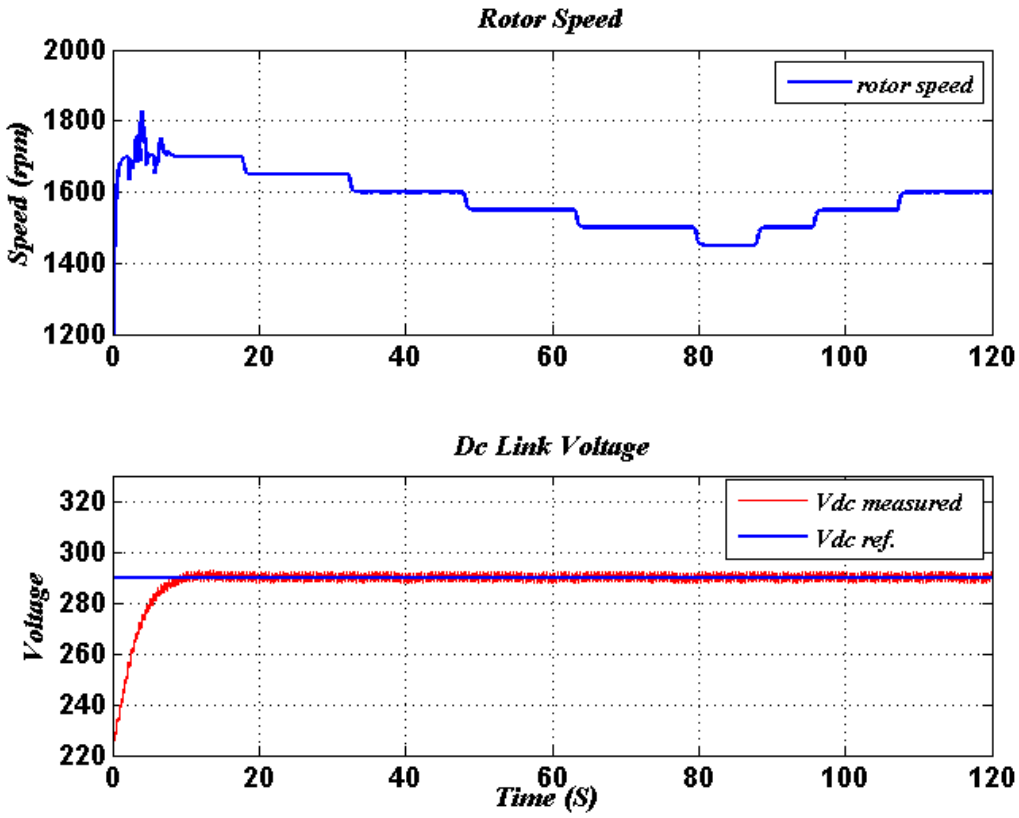

Fig. 4.15a: Dc-link response to parametric mismatches and rotor speed profile changing

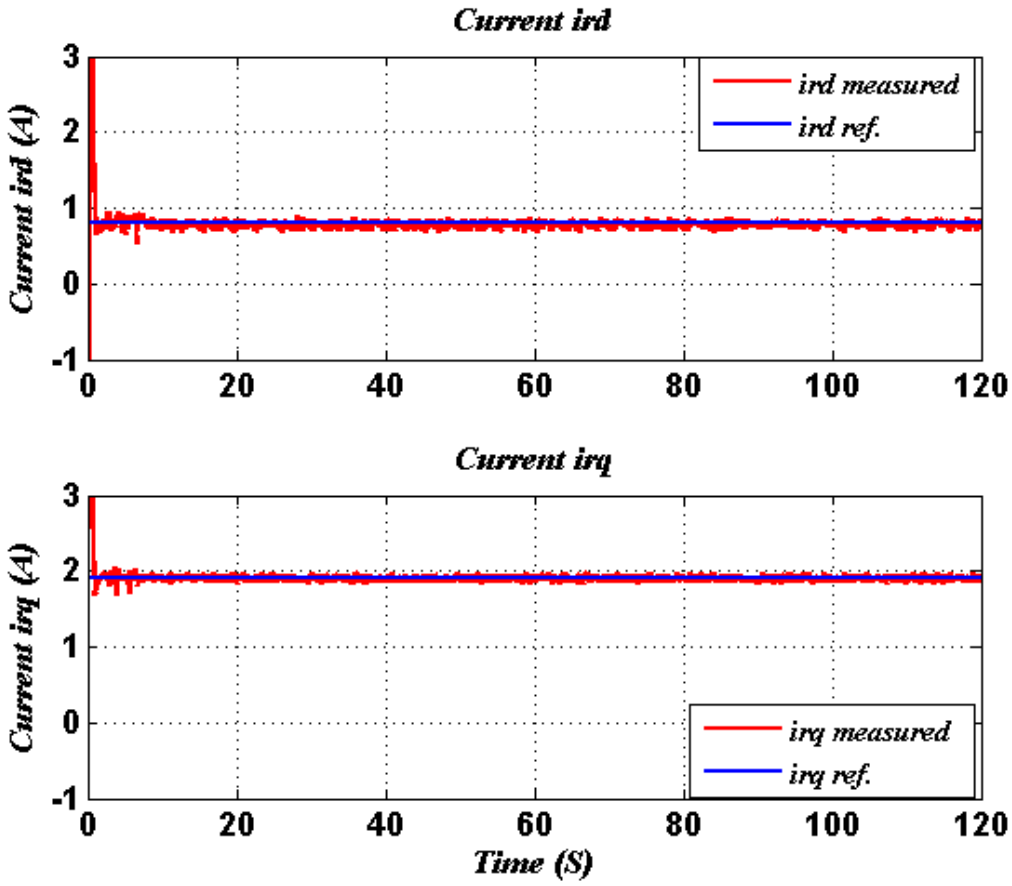

Fig. 4.15a: Rotor current *d-q* response to parametric mismatches and rotor speed profile changing

Chapter 5

Conclusion, Future Work and contribution

A doubly-fed induction generator was introduced in this thesis and a comparison between the doubly-fed machine and other types of wind turbine generator systems with regards to efficiency and output quality was investigated. The equivalent circuits and mathematical models of stator flux-oriented ($\alpha\beta$ and $dq0$) reference frames for the doubly-fed induction generator were illustrated to ascertain the machine's operational behavior. Further, this thesis proposed using a sliding mode control scheme for power central and dc-link voltage regulation of a DFIG-based WECS for total power control. The power control was carried out by controlling the control of the currents at the rotor side, and maintaining the dc-link voltage constant. Under the condition of the stator voltage alignment, the representation of the rotor current state was conducted from the stator and rotor equations of the system. The results demonstrated good performance under various operating conditions as well as robustness to uncertainties, indicating that that the proposed control strategy was experimentally validated.

Future work could involve designing new controllers for a stand-alone system using a DFIG-based wind energy conversion system with a storage method. Also, a new control algorithm could be developed to control the system for rural areas where grid extension is not economically viable. The main obstacles of stand-alone systems are how to control changing load voltage due to unbalanced load demand and frequency variation as the load varies. Therefore, the new controller would have to maintain a constant supply voltage and

frequency, regardless of variations in voltage, and would have to use the battery charging/ discharging operation efficiently when required.

Contribution

- Advanced controllers using SMC approach are proposed and developed to control the power by controlling the rotor current and executed at the laboratory scale 2kW DFIG based wind turbine emulator
- The proposed control strategy has been experimentally validated and the results have shown good performance under different operating conditions and robustness to uncertainties
- Ensured this prototype can be used by graduate student/professional for research and innovation

Table I

Appendix

Quantity	**Value**
DFIG machine	
Power	2 kW
Stator voltage	120 V
Rotor voltage	360 V
Stator current	10 A
Rotor current	3.3 A
Speed	1800 RPM
Pole pairs	2
Ls	0.0662
Lr	*0.0662*
Lm	0.0945
Dynamometer machine	
Required voltage (3 phase)	208 V
Required current (3 phase)	12 A
Speed range	0–3600 RPM
IGBT inverter	
DC-bus voltage	420 V
DC-bus current	10 A
Switching Frequency	0–20 kHz
Grid side controller gains	
Kp = 0.5, Ki = 7, Current regulator = 0.0001 A	
Rotor side controller gains (for i_{dr} and i_{qr})	
Kp = 4.5, Ki = 7.5	

Table II

Gains of the SMC Control Schemes

Quantity	Value
SMC *d-q* current controllers	
k_1,$k_2$$k_3$	4.5, 4.5, 2.3
SMC dc-link voltage controller	
k_1,$k_2$$k_3$	0.3, 0.3, 10^{-4}

Reference

[1] M. Tazil; V. Kumar; R.C. Bansal; S. Kong; Z.Y. Dong; W. Freitas; H.D. Mathur (2010) "Three-phase doubly fed induction generators: An overview.", *IEEE Transaction on Electronic Power*, vol. *4*, pp 75–89.

[2] L. Xu, (2008) "Coordinated control of DFIG's rotor and grid side converters during network unbalance.", IEEE *Transaction on. Power Electron.*, vol. *23*, 1041–1049.

[3] R. Pena, R. Cardenas, J. Proboste, J. Clare, and G. Asher, (2008) "Wind-Diesel Generation Using Doubly Fed Induction Machines", *IEEE Transactions on Energy Conversion*, vol. 23, no. 1, pp. 202-213.

[4] J. Shi, Y. Tang, Y. Xia, L. Ren, and J. Li, (2011) "SMES Based Excitation System for Doubly-Fed Induction Generator in Wind Power Application", *IEEE Transactions on Sustainable Energy*, vol. 21, no. 3, pp. 1105-1108.

[5] A. Merabet, K.T. Ahmed, H. Ibrahim, R. Beguenane, & K. Belmokhtar (2015, May), "Sliding mode speed control for wind energy conversion systems.", In *Electrical and Computer Engineering (CCECE), 2015 IEEE 28th Canadian Conference on* (pp. 1130-1134). IEEE.

[6] R. Pena, J. C Clare, and G. M. Asher, (1996) "Doubly fed induction generator using back-to-back PWM converters and its application to variable speed wind-energy generation", *IEE Transactions on Electronic Power*, Vol. 143, No 3, May 1996.

[7] G. Abad; J. Lopez; M. Rodriguez; L. Marroyo; G. Iwanski, (2011) "Doubly Fed Induction Machine: Modeling and Control for Wind Energy Generation", *IEEE Transaction on Power Electronic*, 2011, 7, pp. 165-175.

[8] A. Merabet, K. T. Ahmed, H. Ibrahim, R. Beguenane, A. M. Y. M. Ghias (2017). Energy management and control system for laboratory scale microgrid based wind-PV-battery, *IEEE Transactions on Sustainable Energy*, vol. 8, no. 1, pp. 145-154.

[9] T. Burton, D. Sharpe, N. Jenkins, and E. Bossanyi, "Wind Energy Hand- book", John Wiley & Sons, Ltd, 2001.

[10] C. Edwards and S. K. Spurgeron," Sliding Mode Control: Theory and Applications." London, U.K.: Taylor & Francis, 1998.

[11] L. Morel, H. Godfroid, A. Mirzaian and J. -. Kauffmann, (1998) "Double-fed induction machine: converter optimisation and field oriented control without position sensor," *IEE Proceedings on Electric Power Applications,* vol. 145, pp. 360-368.

[12] L. Xu and W. Cheng, "Torque and reactive power control of a doubly fed induction machine by position sensorless scheme," *IEEE Transactions on Industry Applications,* vol. 31, pp. 636-646.

[13] Y. Lei, A. Mullane, G. Lightbody, and R. Yacamini, (2006) "Modelling of the Wind Turbine with a Doubly Fed Induction Generator for Grid Integration Studies," *IEEE Transactions on Energy Conversion,* vol. 21, no. 1, pp 145-155.

[14] S.V. Emel'yanov, S.K. Korovin, L.V. Levantovsky, (1986) "Higher-Order Sliding Modes in the Binary Control Systems", *Soviet Physics*, vol. 31, no. 4, pp. 291-293.

[15] H. Sira-Ramirez, (1992) "On the sliding mode control of nonlinear systems," *System and Control Letters,* vol. 19, pp. 303-312.

[16] S.V. Emel'yanov, S.K. Korovin, L.V. Levantovsky, (1986) "Drift Algorithm in Control of Uncertain Processes", *Problems of Control and Information Theory,* vol. 15, no. 6, pp. 425 438.

[17] A. Levant, L.V. Levantovsky,(1993) "Sliding order and sliding accuracy in sliding mode control", *Int. J. of Control,* vol. 58, no. 6, pp. 1247-1263.

[18] B. Beltran, T. Ahmed-Ali, and M. E. H. Benbouzid, (2008) "Sliding mode power control of variable-speed wind energy conversion systems," *IEEE Transaction on. Energy Conversion.*, vol. 23, no. 2, pp. 551–558.

[19] A. Merabet, A. A. Tanvir, K. Beddek (2017). Torque and state estimation for real-time implementation of multivariable control in sensorless induction motor drives, *IET Electric Power Applications*, vol. 11, no. 4, pp. 653-663.

[20] T. Ackermann, L. Söder. (2002) "An overview of wind energy-status ". *Renewable and Sustainable Energy Reviews,* vol. 6, pp. 67-127.

[21] A. Merabet, M. A. Islam, R. Beguenane, and H. Ibrahim, "Second-order sliding mode control for variable speed wind turbine experiment system, *"Renewable. Energy Power*, vol. 12, pp. 1–6, 2014.

[21] Danish Wind Industry Association, Information Available at: /http://www.windpower.org/en/news050214.htm

[23] GL. Johnson, "Wind energy systems.", Englewood Cliffs, NJ: Prentice-Hall Inc.; 1985.

[24] T. Burton, D. Sharpe, N. Jenkins, and E. Bossanyi. "Wind Energy Handbook", John Wiley & Sons, Ltd, 2001.

[25] M. L. Corradini, G. Ippoliti, and G. Orlando, (2013) "Robust control of variable- speed wind turbines based on an aerodynamic torque observer," *IEEE Transaction on. Control System. Technolegy.*, vol. 21, no. 4, pp. 1199–1206.

[26] T. Ghennam. E. M. Berkouk and F. Bruno, (2009) "Modeling and Control of a Doubly Fed Induction Generator (DFIG) Based Wind Conversion System Power Engineering", *Energy and Electrical Drives*, pp. 507-512.

[27] J. Eloy-Garcia, S. Arnaltes and J. L. Rodriguez-Amenedo, (2008) "Direct power control of voltage source inverters with unbalanced grid voltages," *IET Transaction on Power Electronics*, vol. 1, no. 3, pp. 395-407.

[28] H. C. Chen, P. H. Chen, (2014) "Active and Reactive Power Control of a Doubly Fed Induction Generator", *Applied Mathematics & Information Sciences*, vol. 8, No. 1L, pp. 117-124.

[29] M. Suwan, T. Neumann, C. Feltes and I. Erlich, (2012) "Educational experimental rig for Doubly-Fed Induction Generator based wind turbine," *IEEE Transaction on Power and Energy Society General Meeting*, pp. 1-8, 2012.

[30] J. Mohammadi, S. Vaez-Zadeh, S. Afsharnia and E. Daryabeigi, (2014) "A Combined Vector and Direct Power Control for DFIG-Based Wind Turbines," *IEEE Transactions on Sustainable Energy*, vol. 5, no. 3, pp. 767-775.

[31] S. Peresadaa, A. Tillib, A. Tonielli, (2012) "Power control of a doubly fed induction machine via output feedback" *Control Engineering Practice*, vol. 12, pp. 41-57.

[32] K. Ouari, M. Ouhrouche, T. Rekioua, T. Nabil, (2014) "Nonlinear Predictive Control of Wind Energy Conversion System Using DFIG With Aerodynamic Torque Observer", *Journal of ELECTRICAL ENGINEERING*, vol. 65, no. 6, pp. 333–341.

[33] L. H. Hansen, L. Helle, F. Blaabjerg, E. Ritchie, S. Munk-Nielsen, H. Bindner, P.Sorensen, and Bak-Jensen B, (2001)" Conceptual survey of generators and power electronics for wind turbines" ,*Technical Report on National Laboratory*, pp. 145-157.

[34] A Merabet, K.T. Ahmed, H. Ibrahim, R. Beguenane (2016). Implementation of sliding mode control system for generator and grid sides control of wind energy conversion system, *IEEE Transactions on Sustainable Energy*, vol. 7, no. 3, pp. 1327-1335.

[35] V. Akhmatov, (2002) "Variable-Speed Wind Turbines with Doubly-Fed Induction Generators, Part I: Modelling in Dynamic Simulation Tools," *Wind Engineering*, vol 26, no. 2, pp. 1377-1375.

[36] ML.W. Chang, "A MIMO sliding control with second order sliding condition, "*ASME W.A.M.*, paper no. 90-WA/DSC-5, Dallas, Texas, 1990.

[37] B. Beltran, M. E. H. Benbouzid, and T. Ahmed-Ali, (2012) "Second-order sliding mode control of a doubly fed induction generator driven wind turbine," *IEEE Transaction on. Energy Conversion.*, vol. 27, no. 2, pp. 261–269.

[38] C. Evangelista. A. Pisano, P. Puleston, and E. Usai, (2014) "Time-based adaptive second order sliding mode controller for wind energy conversion optimization," *IEE Transaction on conversion*, pp. 2038–2043.

[39] R. C. Bansal, T. S. Bhatti, and D. P. Kothari, (2001) "Some aspects of grid connected wind electric energy conversion systems," *Interdisciplinary Engineering*, vol. 82, pp. 25–

[40] J. M. Mauricio, A. E. LeÓn, A. GÓmez-ExpÓsito and J. A. Solsona, (2008)"An Adaptive Nonlinear Controller for DFIM-Based Wind Energy Conversion Systems," *IEEE Transactions on Energy Conversion*, vol. 23, no. 4, pp. 1025-1035.

[41] W. Cheng and L. Xu, "Torque and reactive power control of a doubly-fed induction machine by position sensorless scheme," *Industry Applications Society Annual Meeting*, vol. 1, pp. 496-502, 1994.

[42] J. C. Y. Hui, A. Bakhshai and P. K. Jain, (2015) "A sensorless adaptive maximum power point extraction method with voltage feedback control for small wind turbines in off-grid applications," *IEEE Journal of Emerging and Selected Topics in Power Electronics*, vol. 3, pp. 817-828.

[43] D. Xiang, L. Ran, P. J. Tavner, S. Yang, (2006) "Control of a Doubly Fed Induction Generator in a Wind Turbine during Grid Fault Ride-Through." On *IEEE Transaction Energy Conversion,* vol. 21**,** pp. 652-662.

[44] P. S. Jesús López, X. Roboam, & L. Marroyo. "Dynamic Behavior of the Doubly Fed Induction Generator During Three-Phase Voltage Dips." On *IEEE Transaction Energy Conversion,* vol. 22, pp.709-717.

[45] L. Xu, & P. Cartwright, (2006) "Direct Active and Reactive Power Control of DFIG for Wind Energy Generation." On *IEEE transaction Energy Conversion,* vol.5**,** pp. 750-758.

[46] A. Luna, F. K. D. A. Lima, D. Santos, P. Rodríguez, E. H. Watanabe, & S. Arnaltes, (2011) "Simplified Modeling of a DFIG for Transient Studies in Wind Power Applications." *IEEE Transaction. on Sustainable Energy*, vol. 58, no. 1, pp 140-160.

[47] J. Hu, H. Nian, H. Xu, & Y. He, (2011) "Dynamic Modeling and Improved Control of DFIG Under Distorted Grid Voltage Conditions." *IEEE transaction on Energy Conversion,* vol. 26, no. 1**, pp.**163-175, 2011.

[48] D. Zhi, L. Xu, & B. W. Williams, (2010) "Model-Based Predictive Direct Power Control of Doubly Fed Induction Generators." *IEEE Transaction. on Power Electron.,* vol. 25, *no*. 2, pp. 341-351.

[49] A. Merabet, A. A. Tanvir, K. Beddek (2016). Speed control of sensorless induction generator by artificial neural network in wind energy conversion system, *IET Renewable Power Generation*, vol. 10, no. 10, pp. 1597-1606.

[50] A. Merabet, M. A. Islam, R. Beguenane, A. M. Trzynadlowski (2015) Multivariable control algorithm for laboratory experiments in wind energy conversion, *Renewable Energy*, vol. 83, pp. 162-170.

[51] A. J. S. Filho, M. E. D. O. Filho, & E. R. Filho, (2011) "A Predictive Power Control for Wind Energy". *IEEE Transaction on Sustainable Energy*, vol. 2, pp. 97-105.

[52] G. Abad, M. Á. Rodríguez, & J. Poza, (2008) "Two-Level VSC Based Predictive Direct Torque Control of the Doubly Fed Induction Machine with Reduced Torque and Flux Ripples at Low Constant Switching Frequency." *IEEE Transaction on Power Electronic.*, vol. 3**,** pp. 1050-1061.

[53] M. Mohseni, & S. Islam, (2010) "A New Vector-Based Hysteresis Current Control Scheme for Three-Phase PWM Voltage-Source Inverters". *IEEE Transaction on Power Electronics*, vol. 9**,** pp. 2299-2309.

[54] M. Mohseni, M. Mesbah, S. Islam, & M.A.S. Masoum, (2011) "Vector-Based Hysteresis Current Regulator for DFIG Wind Turbines under Non-Ideal Supply Conditions". *Australian Journal of Electrical and Electronic Engineering (AJEEE)*, vol.1 pp. 27-38.

[55] S. Z. Chen, N. C. Cheung, K. C. Wong, & J. Wu, (2011) "Integral variable structure direct torque control of doubly fed induction generator. *IET Renewable Power Generation.*, vol. 5**,** pp. 18-25.

[56] G. D. Marques, V. F. A. Pires, S. E. Sousa, & D. M. Sousa, (2011) "A DFIG Sensorless Rotor-Position Detector Based on a Hysteresis Controller". *IEEE Transaction. on Energy Conversion*, vol. 26, pp. 9-17.

[57] B. Shen, B. Mwinyiwiwa, Y. Zhang, & B.-T. Ooi, (2009) "Sensorless Maximum Power Point Tracking of Wind by DFIG Using Rotor Position Phase Lock Loop (PLL). *IEEE Transaction. on Power Electronic,* vol. 24, pp. 942-951.

[58] D. G. Forchetti, G. O. García, & M. I. Valla, (2009) "Adaptive Observer for Sensorless Control of Stand-Alone Doubly Fed Induction Generator". *IEEE Transactions on Industrial Electronics,* vol. 10**,** pp. 4174-4180.

[59] W. Qiao, W. Zhou, J. M. Aller, & R. G. Harley, "Wind Speed Estimation Based Sensorless Output Maximization Control for a Wind Turbine Driving a DFIG". *IEEE Transactions on Power Electronics*, vol.23, no. 3**,** 1156-1169, 2008.

[60] E. Tremblay, S. Atayde, & A. Chandra, (2011) "Comparative study of control strategies for the Doubly Fed Induction Generator in Wind Energy Conversion Systems: a DSP-based implementation approach". *IEEE Transactions on Sustainable Energy,* vol.8, pp.455-470

[61] O. Anaya-Lara, N. Jenkins, J. Ekanayake, P. Cartwright and M. Hughes, Wind Energy Generation, John Wiley & Sons, 2009.

[62] A. Merabet, V. Rajasekaran, A. McMullin, H. Ibrahim, R. Beguenane and J. S. Thongam (2013). Nonlinear model predictive controller with state observer for speed sensorless induction generator–wind turbine systems, *Proc IMechE Part I: Journal of Systems and Control Engineering*, vol. 227, no. 2, pp. 198–213.

[63] B. Wu, Y. Lang, N. Zargari and S. Kouro, Power Conversion and Control of Wind Energy Systems, John Wiley & Sons, 2011. 74] G. Abad, J. Lopez, M. Rodriguez, L. Marryoyo and G. Iwanski, Double Fed Induction Machine, Modeling and Control for Wind Energy Generation, John Wiley & Sons, 2011.

[64] Understanding Renewable Energy Systems, Volker Quaschning, Earthscan, 2005.

[65] Wind Power Electric Systems Modeling, Simulation and Control, Rekioua, Djamila, Springer-Verlag London, 2014

[66] F. Blaabjerg and Z. Chen, Power Electronics for Modern Wind Turbines, Morgan & Claypool Publishers, 2006.

[67] G. Abad, J. Lopez, M. Rodriguez, L. Marroyo, G. Iwanski, (2011) "Doubly Fed Induction Machine: Modeling and Control for Wind Energy Generation", *IEEE Transaction on Sustainable Energy*, vol.13, pp. 2345-2355

[68] R. Pena, J. C. Clare and G. M. Asher, (1996) "Doubly fed induction generator using back-to-back PWM converters and its application to variable-speed wind-energy generation," *IEE Proceedings on Electric Power Applications,* vol. 143, pp. 231-241.

[69] P. Tourou and C. Sourkounis, "Review of control strategies for DFIG-based wind turbines under unsymmetrical grid faults," in *Ecological Vehicles and Renewable Energies (EVER), 2014 Ninth International Conference on,*2014, pp. 1-9.

[70] B. Hopfensperger, D. J. Atkinson and R. A. Lakin, (2000) "Stator-flux-oriented control of a doubly-fed induction machine with and without position encoder," *IEE Proceedings on Electric Power Applications,* vol. 147, pp. 241-250.

[71] Yazhou Lei, A. Mullane, G. Lightbody and R. Yacamini, (2006) "Modeling of the wind turbine with a doubly fed induction generator for grid integration studies," *IEEE Transactions on Energy Conversion,* vol. 21, pp. 257-264.

[72] T. Lei, M. Barnes and M. Ozakturk, (2013) "Doubly-fed induction generator wind turbine modelling for detailed electromagnetic system studies," *IET Renewable Power Generation,* vol. 7, pp. 180-189.

[73] C. E. Ugalde-Loo, J. B. Ekanayake and N. Jenkins, (2013) "State-Space Modeling of Wind Turbine Generators for Power System Studies," *IEEE Transactions on Industry Applications,* vol. 49, pp. 223-232.

[74] A. Tapia, G. Tapia, J. X. Ostolaza and J. R. Saenz, (2003) "Modeling and control of a wind turbine driven doubly fed induction generator," *IEEE Transactions on Energy Conversion,* vol. 18, pp. 194-204.

[75] K.S. Narendra, A.M. Annaswamy, *Stable adaptive systems,* Prentice-Hall, Englewood Cliffs, N J, 1989.

[76] M. Corless, and G. Leitmann, (1981) "Continuous state feedback guaranteeing uniform ultimate boundedness for uncertain dynamic systems," *IEEE Trans. Automatic Control,* vol. 26, pp. 1139-1141.

[77] K. T. Ahmed, A. Merabet, H. Ibrahim, R. Beguenane, (2016), Standalone Wind Energy Conversion System Using OPAL-RT Real-time HIL/RCP Laboratory, *2nd IEEE International Conference on Industrial Informatics and Computer Systems,* Mar. 13-15, Sharjah, UAE, pp. 1-5.

[78] V.I. Utkin, *Sliding modes in control and optimization,* Springer Verlag, Berlin, 1992.

[79] C. Milosavljevic, (1985) "General conditions for the existence of a quasisliding mode on the switching liyperplane in discrete variable systems", *Automation Remote Control,* vol. 43, no. 1, pp. 307-314.

[80]. A. Merabet, KT Ahmed, R Beguenane, H Ibrahim (2015), Feedback linearization control with sliding mode disturbance compensator for PMSG based wind energy conversion system, *IEEE 28th Canadian Electrical and Computer Engineering*, May. 3-6, Halifax, Canada, pp. 1-6.

[81] A. Levant (Levantovsky L.V.), (1993) "Sliding order and sliding accuracy in sliding mode control", *International Journal of Control,* vol. 58, no. 6, pp. 1247-1263.

[82] A.F. *Filippov,Differential Equations with Discontinuous Righthand Side,* Kluwer Academic Publishers, Dordrecht, 1988.

[83] A. Merabet, M. A. Islam, S. Enebeli-Robinson, R. Beguenane (2014). Wind turbine emulator using OPAL-RT Real-time HIL/RCP Laboratory. *26th International Conference on Microelectronics*, Doha, Qatar, Dec. 14-17, 2014, pp. 1-5.

[84] A. Isidori, *Nonlinear control systems*, Springer-Verlag, New York, 1989.

[85] H. Polinder, J. A. Ferreira, B. B. Jensen, A. B. Abrahamsen, K. Atallah, and R. A. McMahon, (2013) "Trends in wind turbine generator systems," *IEEE Transaction on Power Electron.* vol. 1, no. 3, pp.174–185.

[86] I. Munteanu, A. I. Bratcu, N.-A. Cutululis, and E. Ceanga, *Optimal Control of Wind Energy Systems*. London, U.K.: Springer-Verlag, 2007.

[87] A. A Tanvir, A. Merabet, and R. Beguenane, (2015) "Real-time control of active and reactive power for doubly fed induction generator (DFIG)-based wind energy conversion system," *Energies*, vol. 8, no. 9, pp. 10389–10408.

[88] F. Poitiers, T. Bouaouiche, M. Machmoum, (2009) "Advanced control of a doubly-fed induction generator for wind energy conversion," *Electricronic Power Systems Research*, vol. 79, pp. 1085–1096.

[89] R. Cárdenas, R. Peña, S. Alepuz, and G. Asher, (2013) "Overview of control systems for the operation of DFIGs in wind energy applications," *IEEE Transaction Ind. Electron.*, vol. 60, no. 7, pp. 2776–2798.

[90] F. Poitiers, T. Bouaouiche, M. Machmoum, "Advanced control of a doubly-fed induction generator for wind energy conversion," *Electric Power Systems Research*, vol. 79, pp. 1085–1096, 2009.

[91] A. Pisano and E. Usai, "Sliding mode control: A survey with applications in math," *Math. Comput. Simul.*, vol. 81, no. 5, pp. 954–979, 2011.

[92] D. Ginoya, P. D. Shendge, and S. B. Phadke, (2014) "Sliding mode control for mismatched uncertain systems using an extended disturbance observer," *IEEE Transaction on power Electronic*, vol. 61, no. 4, pp. 1983–1992.

[93] A. Merabet, K.T. Ahmed, H. Ibrahim, and R. Beguenane, (2016) "Implementation of sliding mode control system for generator and grid sides control of wind energy conversion system," *IEEE Trans. Sustain. Energy*, vol. 7, no. 3, pp.1327–1335.

[94] F. Valenciaga, and R. D. Fernandez, (2015) "Multiple-input–multiple-output high-order sliding mode control for a permanent magnet synchronous generator wind-based system with grid support capabilities," *IET Renewable Power Generation.*, 2015, vol. 9, no. 8, pp. 925–934.

[95] J. Hu, H. Nian, B. Hu, Y. He, and Z. Q. Zhu, (2010) "Direct active and reactive Power regulation of DFIG using sliding-mode control approach," *IEEE Transaction Energy Conversion*, vol. 25, no. 4, pp. 1028–1039.

[96] O. Barambones, (2012) "Sliding mode control strategy for wind turbine power maximization," *Energies*, vol. 5, pp. 2310–2330.

[97] M. I. Martinez, A. Susperregui, G. Tapia, and L. Xu, (2013) "Sliding-mode control of a wind turbine-driven double-fed induction generator under non-ideal grid voltages," *IET Renewable Power Generation.*, vol. 7, no. 4, pp. 370–379.

[98] B. Beltran, M. E-H. Benbouzid, and T. Ahmed-Ali, (2012) "Second-order sliding mode control of a doubly fed induction generator driven wind turbine," *IEEE Transaction Energy Conversion*, vol. 27, no. 2, pp. 261–269.

[99] C. Evangelista, F. Valenciaga, and P. Puleston, (2013) "Active and reactive power control for wind turbine based on a MIMO 2-sliding mode algorithm with variable gains," *IEEE Transaction Energy Conversion.*, vol. 28, no. 3, pp. 682–689.

[100] A. Susperregui1, M. I. Martinez, G. Tapia, and I. Vechiu, (2013) "Second-order sliding-mode controller design and tuning for grid synchronisation and power control of a wind turbine-driven doubly fed induction generator," *IET Renewable Power Generation*, vol. 7, no. 5, pp. 540–551.

[101] A. Tohidi, H. Hajieghrary, and M. A. Hsieh, (2016) "Adaptive disturbance rejection control scheme for DFIG-based wind turbine: Theory and experiments," *IEEE Transaction Power Electronic*, vol. 52, no. 3, pp. 2006–2015.

[102] K. Kerrouchea, A. Mezouarb, and K. Belgacem, (2013) "Decoupled control of doubly fed induction generator by vector control for wind energy conversion system," *Energy Procedia*, vol. 42, pp. 239–248.

[103] R. Cárdenas, R. Peña, S. Alepuz, and G. Asher, (2013) "Overview of control systems for the operation of DFIGs in wind energy applications," *IEEE Transaction on Power Electronic.*, vol. 60, no. 7, pp. 2776–2798.

[104] O. Barambones, (2012) "Sliding mode control strategy for wind turbine power maximization," *Energies*, vol. 5, pp. 2310–2330.

[105] G. Bartolini, A. Ferrara, E. Usai, (1998) "Chattering Avoidance by Second Order Sliding Mode Control", *IEEE Transaction on Automatic Control*, vol. 43, no. 2, pp. 241-246.

[106] R. Pena, J.C. Clare, GM. Asher, (1996) "Doubly fed induction generator using back-to-back PWM converters and its application to variable-speed wind-energy generation." *IEEE Proceeding Electrical. Power*, vol. *143*, pp.231–241.

[107] Wikipedia, "Real-time simulation," 2013, Available at http://en.wikipedia.org/wiki/Realtime_ simulation.

[108] J. Belanger, P.Venne, and J. N. Paquin, "The What, Where, and Why of Real-Time Simulation," in Planet RT, October 2010.

[109] A. Merabet, K. Ahmed, H. Ibrahim, R. Beguenane, and A. Ghias, "Energy management and control System for laboratory scale microgrid based wind-PV-battery," *IEEE Trans. Sustain. Energy*, vol. 8, no. 1, pp. 145–154, Jan. 2017.